PHYSICAL REVIEW B **96**, 104303 (2017)

Origins of Willis coupling and acoustic bianisotropy in acoustic metamaterials through source-driven homogenization

Caleb F. Sieck,[1,2] Andrea Alù,[1] and Michael R. Haberman[3,2,*]

[1]*The University of Texas at Austin, Department of Electrical and Computer Engineering, Austin, Texas 78712, USA*

[2]*The University of Texas at Austin, Applied Research Laboratories, Austin, Texas 78758, USA*

[3]*The University of Texas at Austin, Department of Mechanical Engineering, Austin, Texas 78712, USA*

(Received 4 March 2017; revised manuscript received 11 August 2017; published 11 September 2017)

Willis fluids, or more generally Willis materials, are homogenized composites that exhibit coupling between momentum and strain. This coupling is intrinsic to inhomogeneous media and can play a significant role in the overall response in acoustic metamaterials. In this paper, we draw connections between bianisotropy in electromagnetism and Willis coupling in elastodynamics to provide a qualitative understanding. Building upon these analogies, we introduce a homogenization technique for acoustic metamaterials based on a source-driven, multiple scattering approach that highlights the physical origins of Willis coupling. Moreover, through numerical examples, we compare several macroscopic material descriptions of acoustic metamaterials with non-negligible Willis coupling. The descriptions neglecting Willis coupling may not satisfy restrictions stemming from reciprocity, passivity, and causality, which suggests that including Willis coupling in macroscopic descriptions is necessary to realize physically meaningful macroscopic parameters.

DOI: 10.1103/PhysRevB.96.104303

I. INTRODUCTION AND MOTIVATION

The emergence of metamaterials in electromagnetism, elastodynamics, and acoustics has provided new impetus for homogenization schemes accounting for multiscale dynamics [1–11]. A valid homogenization scheme must accurately relate the dynamic response of microscopic inhomogeneities and their interactions at the mesoscale to realize metamaterials with exotic macroscopic parameters exhibiting very large, near zero, and even negative values, while also being physically meaningful and independent of the specific setup in which the material is tested [12–14]. One critical result of dynamic homogenization, often neglected due to quasistatic assumptions, is the existence of coupling terms in constitutive relations [6]. The concept of coupled constitutive relations is well known in electromagnetism, and it is generally referred to as bianisotropy or magnetoelectric coupling [15–17]. In contrast, field coupling in elastodynamics and acoustics, commonly referred to as Willis coupling, has only recently begun to receive attention [18,19].

In traditional media, constitutive relations associate fields whose inner product yields either the potential or kinetic energy at a material point. Potential energy is calculated from the inner product of the electric field and electric displacement in electromagnetism, of the stress and strain in elastodynamics, and of the pressure and volume strain in acoustics. Kinetic energy is calculated from the inner product of the magnetic field and magnetic flux in electromagnetism and of the particle velocity and momentum density in elastodynamics and acoustics. Additionally, energy is converted from one form to the other in wave propagation, guided by the differential equations that couple fields related to potential energy and those related to kinetic energy, such as the conservation of momentum.

In bianisotropic or Willis media, however, the constitutive relations are coupled and therefore contain fields associated with both potential and kinetic energy. This coupling between constitutive relations implies energy conversion in the material response to a particular field, which is distinct from the exchange of energy that occurs in wave propagation. Macroscopic coupled constitutive relations may result from multiple microscale and mesoscale effects including chiral inhomogeneities [17,20,21], asymmetric inhomogeneities and substrate effects [5,7,14,22–28], nonlocal effects due to a finite unit cell and multiple scattering [5,9,10,29,30], and in the presence of nonreciprocal biases [15–17,28,31–33].

Despite the prevalence of published work in bianisotropy and Willis coupling, the physical analogies between the origins of these effects in electromagnetic and elastic systems have not been fully discussed. Additionally, while a few works have provided exact theoretical validations of Willis coupling [7,9,25,26], the methods used do not provide a clear picture of the underlying physics. Finally, in order to uniquely define the macroscopic response of an inhomogeneous medium, one must be able to generate fields independently via sources [4–6]. If one attempts to infer the macroscopic response only from free waves (as in most experiments), the resulting parameters are nonunique and may not be physically meaningful [12–14]. This work addresses these considerations by (i) highlighting useful analogies between electrodynamic, elastodynamic, and acoustic systems, (ii) deriving a source-driven, multiple scattering homogenization procedure demonstrating physical origins of Willis coupling in acoustic metamaterials, and (iii) providing numerical examples demonstrating that Willis coupling must be taken into account in order for macroscopic parameters to be physically meaningful.

This work is organized as follows. Section II provides a brief perspective on the connection between bianisotropy in electromagnetism and Willis coupling in elastodynamics and acoustics, highlighting important physical analogies and qualitative examples. The remainder of this work focuses on Willis coupling in acoustic metamaterials, which was inspired and guided by the analogous work in electromagnetism, particularly the works of Alù [5] and Simovski [12]. In

*haberman@utexas.edu

Sec. III, a source-driven, multiple scattering homogenization procedure for acoustic metamaterials provides an intuitive demonstration of the origins of macroscopic coupling in acoustic metamaterials. The homogenization procedure results in exact solutions for one-dimensional (1D) periodic media, which are discussed in detail in Sec. IV. Due to the nonuniqueness of macroscopic parameters in the absence of sources, the derived *effective* parameters are compared to two additional macroscopic descriptions that one might propose to model free waves in the metamaterial: *equivalent* parameters which neglect Willis coupling, and *Bloch* parameters which relate microscopic fields rather than effective fields. Three example 1D periodic media are considered, and the *effective*, *equivalent*, and *Bloch* parameters are discussed in light of physical restrictions on values.

II. BIANISOTROPY AND WILLIS COUPLING

This section provides an introduction to bianisotropy in electromagnetism and analogous effects in acoustic/elastic wave systems and qualitatively demonstrates field coupling using fundamental physics. Section II A provides a brief introduction and history of the known physical mechanisms leading to macroscopically observable bianisotropy in electromagnetism and an example of how bianisotropy may be introduced at the microscale by an asymmetric inhomogeneity. Section II B provides an overview of work in elastodynamics and acoustics involving coupled constitutive relations, an example of a coupled response from an asymmetric inhomogeneity in an acoustic pressure field, and a qualitative discussion of nonlocal coupling. Finally, Sec. II C reviews the general restrictions on macroscopic material parameters through the expressions of reciprocity, passivity, and causality in homogeneous acoustic media [14].

In order to clarify the discussion, the authors tried to use common variables in each of the disciplines: electromagnetism, elastodynamics, and acoustics. As such, variables only in Sec. II A will refer to the electromagnetic definitions; variables only in Sec. II B will refer to elastodynamics; and variables in the remainder of this work will refer to acoustic definitions provided wherever defined. Additionally, the forms of the constitutive relations presented in Eqs. (1), (3), and (4) were chosen based on convenience of comparison and tradition, rather than being expressed in terms of the primary fields of their corresponding disciplines [34,35].

A. Bianisotropy in electromagnetism

The study of bianisotropic media in electromagnetism has a long history, with inquiry stretching back over 200 years [17,20]. The term "bianisotropic" was proposed in 1968 by Cheng and Kong [15] to describe a material that displays an electrical response resulting from both electric and magnetic excitation and a magnetic response resulting from both magnetic and electric excitation and, in general, the response is not parallel to either excitation. This behavior is represented by the constitutive relations provided in Eq. (1). A variety of physical effects may be efficiently modeled in the frequency domain using bianisotropic constitutive relations, and knowledge of their origins provides key insight into understanding the so-called Willis coupling in elastodynamics and acoustics.

The general bianisotropic constitutive relations in electromagnetism can be expressed in indical notation as

$$\begin{aligned} D_i &= \epsilon_{ij} E_j + \zeta_{ij} H_j, \\ B_i &= \xi_{ij} E_j + \mu_{ij} H_j, \end{aligned} \tag{1}$$

where the electric and magnetic field strengths, $\boldsymbol{E}$ and $\boldsymbol{H}$, and the electric and magnetic displacements, $\boldsymbol{D}$ and $\boldsymbol{B}$, are all vectors, and the four material parameters, electric permittivity $\underline{\boldsymbol{\epsilon}}$, magnetic permeability $\underline{\boldsymbol{\mu}}$, and two coupling parameters $\underline{\boldsymbol{\zeta}}$ and $\underline{\boldsymbol{\xi}}$, are all second-order tensors. Restrictions on the parameter tensors based on symmetry, time, and spatial inversion, reciprocity, and passivity were formally expressed by Kong [16].

The earliest observed effect that can be modeled with bianisotropic constitutive relations dates back more than 200 years and is known as optical activity [17,20]. This phenomenon occurs naturally in some crystals and is marked by the rotation of linearly polarized light as it propagates through a material [17,20]. Media with optical activity are reciprocal, and materials demonstrating this response are generally referred to as chiral media. (An often used alternative formalism of optical activity presents the electric displacement as a function of the electric field and its curl [36].) In the mid-20th century, it was shown that certain magnetic materials exhibit magnetization proportional to electrical excitation. This became known as the magnetoelectric effect, and it is nonreciprocal [17]. Both of these effects were demonstrated in engineered materials in the first half of the 20th century, chirality by Lindman in 1914 using subwavelength microstructures composed of copper helices [37] and the magnetoelectric effect by Tellegen in 1948 using the nonreciprocal circuit element he called a gyrator [31]. Propagation in general bianisotropic media continued to be studied extensively throughout the second half of the 20th century [17,20].

For propagation in isotropic media with magnetoelectric coupling (known as bi-isotropic media), all the material parameters presented in Eq. (1) can be represented by scalars, and the coupling coefficients take the form

$$\begin{aligned} \zeta &= \kappa^{\mathrm{nr}} + \kappa^{\mathrm{or}} + i\kappa^{\mathrm{er}}, \\ \xi &= \kappa^{\mathrm{nr}} + \kappa^{\mathrm{or}} - i\kappa^{\mathrm{er}}. \end{aligned} \tag{2}$$

In these expressions, κ^{er} contains the chirality of the medium, and κ^{nr} contains the nonreciprocal magnetoelectric effect, also known as the Tellegen parameter. More generally, κ^{nr} describes coupling due to many other nonreciprocal effects including modeling moving media in a stationary reference frame and time-varying media [15,16]. In contrast, κ^{er} contains contributions from coupling mechanisms which are even in wave vector and reciprocal, hereafter referred to as even coupling. In addition to chirality, even coupling mechanisms common in metamaterials include substrate effects [23] and asymmetric microstructures such as split-ring resonators and Ω particles [22]. The third parameter contributing to coupling, κ^{or}, accounts for reciprocal effects which are odd in wave vector, hereafter referred to as odd coupling. κ^{or} was recently demonstrated to occur in periodic lattices, and it is due to the finite phase velocity over a unit cell and multiple scattering

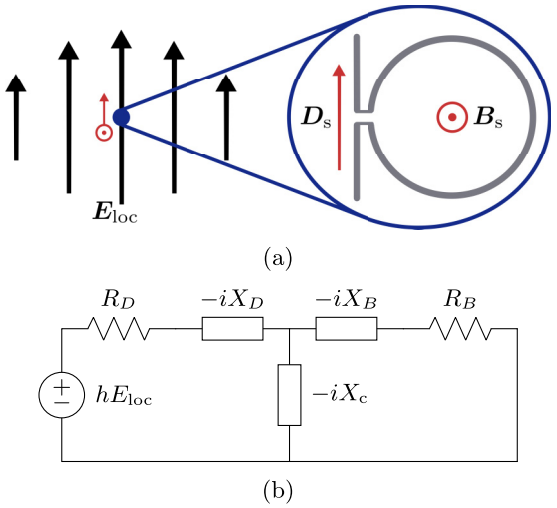

FIG. 1. Ω particle demonstrating a microscopic origin of even coupling κ^{er} in electromagnetism. (a) A perfectly conducting Ω particle with height h produces electric $\boldsymbol{D}_s$ and magnetic $\boldsymbol{B}_s$ dipole scattering when located at a local electric field $\boldsymbol{E}_{loc}$ maximum and magnetic field null. (b) The operation of the Ω particle may be explained by its equivalent circuit [38,39], where the response of the arms is modeled with reactance X_D, the response of the loop by X_B, and the coupling between the arms and loop by X_c. The resistances represent the scattered fields by the electric R_D and magnetic R_B dipoles due to the excitation by the local electric field and current around the loop.

effects, i.e., nonlocal effects, which will be discussed here as mesoscale effects. A major result of these findings is that neglecting κ^{or} in the homogenization of periodic arrays can result in effective properties that do not satisfy the restrictions imposed by passivity and causality on the response of a material when subjected to external fields [4,5,13].

As mentioned above, asymmetric microstructures can lead to bi(an)isotropy at the macroscale. Since microstructural asymmetries lead to bianisotropy in electromagnetic metamaterials, which this paper will show has an acoustic analog, it is informative to introduce an example physical response at the microscale leading to coupled field behavior. One such structure is the so-called Ω particle [22], which is illustrated in Fig. 1(a) and described here. Given a perfectly conducting, Ω-shaped microstructure located at a local electric field $\boldsymbol{E}_{loc}$ maximum and magnetic field null, the microscopic particle responds like the RLC circuit shown in Fig. 1(b), where the reactances X_D, X_B, and X_c are provided in Refs. [38,39]. The local electric field induces a charge separation, or a voltage source hE_{loc}, in the arms of the Ω particle that respond as a perfectly conducting rod of length h modeled by X_D. The charge separation in turn results in a current around the loop, which may be modeled by X_B, and X_c models the coupling between the arms and loop. Energy is dissipated through reradiation in the form of a scattered electric dipole $\boldsymbol{D}_s$ along the arms and a scattered magnetic dipole $\boldsymbol{B}_s$ through the loop due to the time-varying current. These two forms of radiation are represented by red vectors in Fig. 1(a) and as the resistances R_D and R_B in Fig. 1(b). In this manner, a microscopic particle may have a magnetic response to an electrical stimulus or an electric response due to a magnetic stimulus, i.e., the Ω particle may be excited by an incident magnetic field through the loop. Because this microstructure partially converts a stimulus of potential (kinetic) energy to a kinetic (potential) response, an inhomogeneous medium composed of many such subwavelength microstructures embedded in a background medium will exhibit macroscopic field coupling represented by constitutive relations with the form of Eq. (1) [22].

In electromagnetism, materials are characterized by their electric and magnetic responses, which are coupled in the case of bianisotropic media. The analogous responses in elastodymanics correspond to relations between stress and strain and between velocity and momentum. In the following, a class of materials known as Willis media will be discussed, which are analogous to bianisotropic media due to coupling between stress-strain and momentum-velocity relations [19].

B. Willis coupling in elastodynamics and acoustics

In the 1960s, several groups independently proposed that "acoustical activity" (analog to optical activity) would exist in noncentrosymmetric crystals [40–43]. This effect was measured in α quartz by Pine in 1970 [44], and acoustic chirality was later proposed and demonstrated in engineered composites in the 1980s [20,21]. Chirality, which requires that the medium support transverse wave propagation with rotationally polarized fields, can only occur in elastic media, but will be absent in fluids which only support longitudinal motion. In mechanics, the term chirality also often refers to the related static effect whereby a uniform strain results in a torque, and chiral geometries can be used to achieve a negative Poisson's ratio [45]. Additionally, chiral elements have recently been used as spiral phase plates to produce acoustic orbital momentum [46], in which case the emergent acoustic beam from the plate has an azimuthal dependence, but the wave motion is still longitudinal.

Apart from the studies of chirality, Willis demonstrated in the 1980s that field coupling is a general result of dynamic homogenization of inhomogeneous media [18,47,48]. A surprising result of Willis' work was the prediction of coupled constitutive relations in the form of Eq. (3) for both transverse and longitudinal waves, regardless if media supports rotational fields [1,19,24]. This coupling as a result of dynamic homogenization has therefore come to be referred to as Willis coupling. Given that fluids only support longitudinal waves, one must therefore conclude that the analog of bianisotropic coupling exists in fluid acoustics. Recent work by Milton and Willis [19] outline the development of Willis' theory, and a recent review by Srivastava [49] highlights much of the work thus far in this area.

The so-called Willis constitutive relations are generally presented as

$$\begin{aligned} \sigma_{ij} &= C_{ijkl}\varepsilon_{kl} + S_{ijk}\dot{\xi}_k, \\ \mu_i &= \tilde{S}_{ijk}\varepsilon_{jk} + \tilde{\rho}_{ij}\dot{\xi}_j, \end{aligned} \tag{3}$$

where the Cauchy stress tensor $\underline{\boldsymbol{\sigma}}$ is proportional to not only the infinitesimal strain tensor $\underline{\boldsymbol{\varepsilon}}$ via the fourth-order stiffness tensor $\boldsymbol{\mathcal{C}}$ but also to the time derivative of the displacement vector $\dot{\boldsymbol{\xi}}$ via a third-order coupling tensor $\mathcal{S}$. Similarly, the

momentum density vector $\boldsymbol{\mu}$ is also proportional to the strain via a third-order coupling tensor $\tilde{\mathcal{S}}$ and the time derivative of the displacement vector via the mass density tensor $\underline{\tilde{\boldsymbol{\rho}}}$ [1,19]. The general result provided by Willis was that dynamic homogenization leads to coupled constitutive relations with material properties that are temporally and spatially dispersive [1,6,19]. Recent work by Nassar *et al.* [26] provides a detailed account of the necessary conditions for the application of Willis' homogenization theory to periodic media.

For 1D propagation, the constitutive parameters $\mathcal{C}$, $\mathcal{S}$, $\tilde{\mathcal{S}}$, and $\underline{\tilde{\boldsymbol{\rho}}}$ reduce to scalars C, S, $\tilde{S}$, and $\tilde{\rho}$, and for periodic media that are lossless and reciprocal, the coupling coefficients have been shown to be related by $\tilde{S} = -\mathrm{conj}(S)$ for purely longitudinal propagation [25], purely shear propagation [7], and discrete systems [26] [note that constitutive relations in references may be in a complementary form compared to Eq. (3), which will result in slightly different expressions for $\mathcal{C}$, $\mathcal{S}$, $\tilde{\mathcal{S}}$, and $\underline{\tilde{\boldsymbol{\rho}}}$]. This is consistent with the relation between the even and odd reciprocal coupling parameters κ^{er} and κ^{or} in Eq. (2). Additionally, Nemat-Nasser and Srivastava [25] noted that $\mathrm{Im}(S)$ is only nonzero when the unit cell is asymmetric and that $\mathrm{Re}(S)$ is finite (except in the static limit) regardless of unit-cell symmetry. It has recently been demonstrated that $\mathrm{Re}(S)$ in lossless composites is due to nonlocal effects and has been shown to exist in periodic media with symmetric unit cells in 1D [29] and 2D [30] for acoustics and in 2D [9] for elastic waves. This work will show that for lossless composites $\mathrm{Im}(S)$ is due to asymmetric microstructures (even coupling) and $\mathrm{Re}(S)$ is the result of mesoscale effects associated with the finite phase velocity across the unit cell and multiple scattering in the lattice (odd coupling).

Independent of the works discussing Willis coupling, Koo *et al.* [27] recently demonstrated numerically and experimentally the use of acoustic bianisotropy to impedance match waveguides with different cross-sectional areas and to independently control reflection and transmission angles from a metasurface with a normally incident plane wave. Their demonstrations provide the first experimental evidence of acoustic bianisotropy and were inspired by the analogs to bianisotropy in electromagnetism. The experimental demonstrations were recently explained in terms of Willis coupling by Muhlestein *et al.* [50] who provided detailed theoretical and experimental evidence of Willis coupling in a small asymmetric metamaterial sample. Also independently, Shui *et al.* [32] demonstrated nonreciprocal coupling for elastic waves using a layered medium with time-varying properties, which appears to be analogous to nonreciprocal coupling κ^{nr} in electromagnetism, though it was not described in this manner. A similar effect was recently discussed by Nassar *et al.* [33] who explained the effect as nonreciprocal Willis coupling. Moving elastic media may also be represented as a medium with nonreciprocal Willis coupling in a stationary reference frame [28].

The frequency domain coupled constitutive relations for fluid acoustics may be expressed as

$$\begin{aligned} \boldsymbol{\mu} &= \underline{\boldsymbol{\rho}} \cdot \boldsymbol{u} - \boldsymbol{\eta} p, \\ \varepsilon &= \boldsymbol{\gamma} \cdot \boldsymbol{u} - \beta p, \end{aligned} \tag{4}$$

where vector fields are momentum density $\boldsymbol{\mu}$ and acoustic particle velocity $\boldsymbol{u}$ and scalar fields are volume strain ε and acoustic pressure p. The fields are related by the anisotropic mass density tensor $\underline{\boldsymbol{\rho}}$, adiabatic compressibility scalar β, and coupling vectors $\boldsymbol{\eta}$ and $\boldsymbol{\gamma}$. Consistent with the origins of bianisotropy in electromagnetism presented in Eq. (2) and the observation that $\tilde{S} = -\mathrm{conj}(S)$ in reciprocal, lossless, 1D elastodynamic studies [7,25,26], this work demonstrates that for reciprocal fluids

$$\begin{aligned} \boldsymbol{\eta} &= \boldsymbol{\chi}^{\mathrm{o}} + i\boldsymbol{\chi}^{\mathrm{e}}, \\ \boldsymbol{\gamma} &= \boldsymbol{\chi}^{\mathrm{o}} - i\boldsymbol{\chi}^{\mathrm{e}}, \end{aligned} \tag{5}$$

where $\boldsymbol{\chi}^{\mathrm{o}}$ is odd coupling, i.e., odd in wave vector $\boldsymbol{k}$ such that $\boldsymbol{\chi}^{\mathrm{o}}(\boldsymbol{k}) = -\boldsymbol{\chi}^{\mathrm{o}}(-\boldsymbol{k})$, and $\boldsymbol{\chi}^{\mathrm{e}}$ is even coupling, i.e., even in wave vector $\boldsymbol{k}$ such that $\boldsymbol{\chi}^{\mathrm{e}}(\boldsymbol{k}) = \boldsymbol{\chi}^{\mathrm{e}}(-\boldsymbol{k})$.

In Eq. (4), the momentum density and volume strain have been expressed in terms of acoustic particle velocity and pressure, as opposed to being a limiting case of Eq. (3) as was discussed in Ref. [14]. Therefore, the dynamic mass density tensors $\underline{\tilde{\boldsymbol{\rho}}}$ and $\underline{\boldsymbol{\rho}}$ in Eqs. (3) and (4), respectively, are slightly different parameters. $\underline{\tilde{\boldsymbol{\rho}}}$ is the dynamic density one would measure if inertial effects were determined with the sample held at constant strain, whereas $\underline{\boldsymbol{\rho}}$ is the dynamic density of the same measurement but with the sample under constant pressure.

Although elastic material behavior is often described using the kinematic field (usually $\boldsymbol{\xi}$) as the independent variable, the independent variable in acoustics is often assumed to be the pressure p. The difference is clearly illustrated by the fact that the wave equations for elastic media and fluids are usually derived for $\boldsymbol{\xi}$ and p, respectively. This follows from the natural description of the physical processes underlying wave motion in elastic and fluid media. Stress is assumed to be related to strain via Hooke's law in linear elasticity through an idealized quadratic strain energy density function (rather than a stress energy density function), but in fluids, the pressure variations are related to changes in density via thermodynamic relations (isentropic pressure variations). The description of wave propagation in terms of volume strain as a dependent field of the pressure via the compressibility $\beta = \rho_0^{-1}\partial\rho/\partial p|_{s=0}$ is therefore the more natural representation for acoustic waves. Additionally, the formulation presented in Eq. (4) is more convenient for the homogenization derviation in Sec. III and is directly analogous to the commonly used $E - H$ form of electromagnetism presented in Eq. (1). However, despite the convenience and tradition, we note that $\boldsymbol{E}$ and $\boldsymbol{B}$ are actually the fundamental fields in electromagnetism [34], and fluctuating enthalpy has been suggested as the fundamental acoustic field [35].

As discussed in the previous section, coupling in electromagnetism occurs between electric and magnetic material responses, two distinct phenomena. The origins of coupling in acoustics and elastodynamics are not as obvious because all the fields are thermodynamic in nature; however, the origins become more evident from the acoustic constitutive relations [Eq. (4)]. In the absence of coupling, i.e., $\boldsymbol{\gamma} = \boldsymbol{\eta} = 0$, the first expression of Eq. (4) is the definition of momentum, a vector equation representing purely translational motion at a vanishingly small material point. The velocity and momentum density at this field point are related to the local kinetic energy. A particle demonstrating this type of motion is associated with

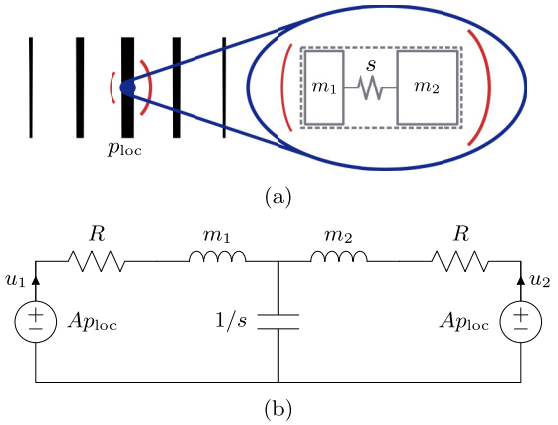

FIG. 2. Asymmetric acoustic inhomogeneity demonstrating the microscopic origin of even coupling. (a) Inhomogeneity with cross-sectional area A consisting of two masses m_1 and m_2 separated by a spring with stiffness s and located at a local acoustic pressure maximum and particle velocity null. (b) Equivalent circuit model demonstrating that the local pressure acts as force sources Ap_{loc} in series with the masses m_1 and m_2, separated by the compliance $1/s$. The resistors R represent the scattered acoustic field due to the motion of the masses. For $m_1 \neq m_2$, $u_1 \neq u_2$ implying that the inhomogeneity response is not purely monopolar despite the monopole nature of the source. Thus, the scattered wave will contain monopole and dipole components.

acoustic dipolar radiation and is therefore often referred to as a dipole. Similarly, in the absence of coupling, the second expression of Eq. (4) is a Hookean relation and the equation of state for an isentropic fluid, which is a scalar equation representing purely compressional motion at a vanishingly small material point. The pressure and volume strain at this field point are related to the local potential energy. A particle demonstrating this type of motion is associated with acoustic monopolar radiation and is therefore often referred to as a monopole. It is the coupling between *monopole* and *dipole* motion at the microscale and/or mesoscale of inhomogeneous fluids that leads to macroscopic Willis constitutive relations.

In the previous section, it was demonstrated that macroscopic even coupling can result from the asymmetry present in microscopic inhomogeneities such as Ω particles due to their coupled scattering. Even coupling has been demonstrated in Willis media using systems of unequal masses and springs [14,28,51]. It is shown here that inhomogeneities consisting of unequal masses separated by a spring produce the analogous effect of Ω particles. An asymmetric acoustic inhomogeneity and equivalent circuit are presented in Fig. 2. Consider a microscopic inhomogeneity with cross-sectional area A consisting of two masses m_1 and m_2, separated by an ideal spring with stiffness s, and located at a local acoustic pressure maximum and particle velocity null as shown in Fig. 2(a). Scattered acoustic waves, represented by red curves, will radiate from both masses. Since a pressure maximum coincides with a particle velocity null, i.e., $\boldsymbol{u}_{\mathrm{loc}} = 0$, then the local field imposes a purely monopole excitation. The monopolar excitation is indicated by force sources in series with the masses and in parallel with the compliance $1/s$ as shown in the equivalent circuit in Fig. 2(b). In the equivalent circuit, the velocities of the masses are labeled as u_1 and u_2, which are positive for the masses moving towards each other with positive pressure, and the resistances R represent the acoustic field radiated into the background fluid from the motion of the masses. Purely monopolar motion of the inhomogeneity requires $u_1 = u_2$, and purely dipolar motion of the inhomogeneity requires $u_1 = -u_2$. From the equivalent circuit, for a monopole excitation and $m_1 \neq m_2$, the inhomogeneity responds with a combination of monopolar and dipolar motion because $u_1 \neq u_2$ and $u_1 \neq -u_2$. This simple model demonstrates the origins of even coupling at the microscale due to the presence of asymmetric microscopic inhomogeneities. An inhomogeneous medium consisting of many such microstructures will exhibit some amount of coupling in effective parameters as in Eqs. (3) and (4).

While even coupling can originate from asymmetry at the microscale, odd coupling arises at the mesoscale. For example, consider an array of inhomogeneities with feature size l and periodicity L in a background fluid with wave number $k_0 = \omega/c_0 = 2\pi/\lambda_0$. Dispersion of the acoustic waves propagating in this array can be described with the macroscopic wave number $k = \omega/c = 2\pi/\lambda$. Even though the inhomogeneity may indeed be small compared to the wavelength in the background media, the phase change over a unit cell may be significant due to resonances, i.e., even though $k_0 l < 0.1$ in many cases $kL > 1$, which is often the case for metamaterials with $c \to 0$, because for $c \to 0$ then $\lambda \to 0$ at finite frequency. The finite phase change over the distance of a unit cell, i.e., $kL > 0$, demonstrates that there is an exchange between kinetic and potential energy due to effective wave propagation over the finite unit cell. In the macroscopic constitutive relations, the phase change leads to odd coupling, odd because the phase change over the unit cell will change sign with the opposite propagation direction. This provides a qualitative argument for considering odd coupling, which quantifies the exchange between monopolar and dipolar motion due to finite phase change over the length of the unit cell. Odd coupling becomes particularly profound in slow phase speed metamaterials. As c tends to zero, so does λ, and when λ becomes comparable to L, the macroscopic description of the inhomogeneous medium as a single homogeneous material with effective properties begins to lose physical meaning. The mesoscopic origins of odd coupling are demonstrated in the homogenization procedure derived in Sec. III, and the impact of neglecting odd coupling in 1D examples is discussed in Sec. IV.

Sections II A and II B have provided an overview and simple examples illustrating the physical basis for coupled constitutive relations. The next section provides motivation for considering these more general constitutive relations based on the desire for physically meaningful macroscopic descriptions of inhomogeneous media.

C. Physically meaningful macroscopic parameters

The purpose of the previous sections was to provide a background on the development and use of bianisotropy and Willis coupling and to provide analogies between the behavior in electromagnetic and elastic systems. In addition to understanding the origins of these coupling terms, a primary motivation for this work is to derive macroscopic material parameters that satisfy restrictions based on passivity, causality,

and reciprocity for homogenized systems. These restrictions have received considerable attention in electromagnetism [12,13,16], and recent work by Muhlestein *et al.* [14] derived restrictions for Willis solids with even coupling and considered the implications of these restrictions for acoustics as a special limit of elastodynamics. Here, only restrictions on the acoustic parameters introduced in Eqs. (4) and (5) are reviewed.

Reciprocity requires symmetry in the mass density tensor $\rho_{ij} = \rho_{ji}$, if it has a local response. It also requires that the coupling parameters take the form of Eq. (5) when odd and even components are considered. If the medium can be assumed to be reciprocal and passive, restrictions on the imaginary parts of material parameters are also imposed. The imaginary parts of the mass density and compressibility must satisfy

$$\mathrm{Im}(\rho_{ij}) \geqslant 0, \quad \mathrm{Im}(\beta) \geqslant 0, \tag{6}$$

when using the $e^{-i\omega t}$ time convention, which is used throughout this work. Passivity also places restrictions on the magnitude of the imaginary parts of $\boldsymbol{\chi}^{\mathrm{o}}$ and $\boldsymbol{\chi}^{\mathrm{e}}$ [14,52].

Additionally, causality dictates that in a frequency band with negligible loss and away from resonances,

$$\partial\rho_{ij}/\partial\omega \geqslant 0, \qquad \partial\beta/\partial\omega \geqslant 0. \tag{7}$$

Although consistent with electromagnetism [12,13,53], this is nonintuitive since usually in elastodynamics and acoustics one is confronted with a relaxing media for which $\partial\beta/\partial\omega \leqslant 0$. The two limiting cases of low-loss media with resonances and relaxing media are discussed in detail by Muhlestein *et al.* [14]. Generally, low losses are assumed in metamaterial models and applications, so the inequalities in Eq. (7) are valid away from resonances.

It is important to note that metamaterial parameters are often reported that do not satisfy the restrictions presented in Eqs. (6) and (7), yet the combination of these parameters in the characteristic impedance and wave number demonstrate passive and causal energy propagation. In Sec. IV, we discuss the extraction of the wave impedance $Z = \sqrt{\rho_{\mathrm{eq}}/\beta_{\mathrm{eq}}}$ and wave number $k = \omega\sqrt{\rho_{\mathrm{eq}}\beta_{\mathrm{eq}}}$ from an inhomogeneous sample, which has been modeled as being *equivalent* to a homogeneous fluid with parameters ρ_{eq} and β_{eq}. Such a model does not consider Willis coupling. If the sample is reciprocal and passive, the extracted Z and k should be chosen such that they satisfy passivity and causality. However, this does not guarantee that ρ_{eq} and β_{eq} will satisfy Eqs. (6) and (7), and if coupling is present one (or both) of the *equivalent* parameters will likely not satisfy passivity and causality. Because Z and k satisfy passivity and causality, it is a model that can still capture the wave motion, but the homogenized properties lose physical meaning, giving the appearance of local gain even when all of the constituents are purely passive.

Koschny *et al.* [54] pointed out in electromagnetism that, due to nonlocal effects, antiresonant behavior was observed in extracted metamaterial properties which violated passivity. Later, it was shown that the nonlocal effects could be accounted for with bianisotropy [4], and Alù discussed the relation between neglecting bianisotropy and acausal metamaterial properties [5,13]. If one wishes to describe the overall response of inhomogeneous acoustic and elastic media with macroscopic parameters, it is necessary that the resulting macroscopic parameters strictly obey reciprocity, causality, and passivity on their own, rather than in combination. This is one of the primary motivations of this work, and the implications of the model developed in Sec. III on these restrictions will be explored further in Sec. IV C for 1D lattices.

III. HOMOGENIZATION PROCEDURE

Acoustic wave propagation is described through the appropriate application of the Navier-Stokes equation (conservation of momentum), the continuity equation (conservation of mass), entropy equation (internal energy), and an equation of state (constitutive equation) [55]. For a linear, locally reacting fluid, the conservation of momentum expression simplifies to

$$\nabla p = -\dot{\boldsymbol{\mu}} + \boldsymbol{f}. \tag{8}$$

In this expression, the scalar p represents the acoustic pressure. The vector $\boldsymbol{\mu} = \rho_0\boldsymbol{u}$ is the momentum density with ρ_0 representing the density of the fluid supporting the acoustic wave and the vector $\boldsymbol{u}$ representing the acoustic particle velocity, and the overdot represents the time-derivative operation. The vector $\boldsymbol{f}$ represents body forces, which can also be described as dipole sources, at the point of evaluation.

The linearized form of the continuity equation is usually expressed as $\partial\rho/\partial t = q - \rho_0\nabla\cdot\boldsymbol{u}$ [55], where ρ is the instantaneous density and q represents volume, or monopole, sources. However, from an analysis of strain rate on a volume element, Hunt [56] demonstrated that

$$\nabla\cdot\boldsymbol{u} = \dot{\varepsilon} + q \tag{9}$$

is an equivalent form of the equation of continuity, where ε is the volume strain (dilatation [56]). For linear acoustics, volume strain is proportional acoustic pressure via a Hookean relation $\varepsilon = -\beta_0 p$. Here, β_0 is the adiabatic compressibility of the fluid and the inverse of the bulk modulus.

This section outlines a source-driven homogenization theory based on multiple scattering modeled after analogous work in electromagnetism [5]. It differs from previous acoustic multiple scattering homogenization approaches, e.g., Twersky [57,58] and Torrent and Sánchez-Dehesa [59] and references therein, by taking a source-driven approach, which is necessary to guarantee a unique effective response through independently imposed pressure and velocity fields [4–6], and by allowing for coupling between monopole and dipole responses. The homogenization procedure will be introduced as follows. In Sec. III A, equations of conservation of momentum (8) and mass (9) will be used to determine *microscopic* and *macroscopic* fields due to a source distribution with an $e^{i\boldsymbol{k}\cdot\boldsymbol{x}}e^{-i\omega t}$ dependence, with and without inhomogeneities. In Sec. III B, *macroscopic* effective fields will be related to the scattering properties of inhomogeneities (*microscopic* effects). The relation of *macroscopic* fields to *mesoscopic* effects due to finite phase velocity along the array and inhomogeneity interaction from multiple scattering will be introduced in Secs. III A and III C, respectively. The responses of the inhomogeneities, their long-range interaction, and finite unit-cell effects will be expressed in terms of monopole, dipole, and coupled coefficients. The homogenized, *effective* material parameters will be explicitly solved for in the cases

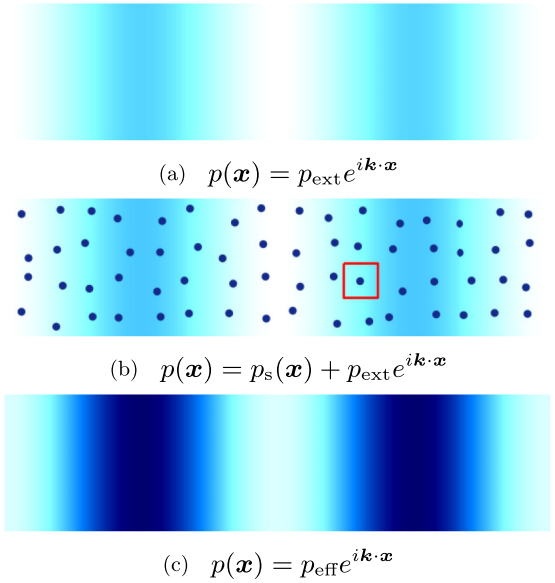

FIG. 3. Conceptual illustration of source-driven homogenization procedure: (a) background fluid with externally controlled body forces and volume velocity sources imposing an arbitrary $(\omega,\boldsymbol{k})$ pair. (b) The introduction of inhomogeneities result in a total field that is a combination of scattered and externally imposed fields. The scattered fields are not shown to minimize clutter, and the unit cell analyzed in Sec. III is denoted by the red box. (c) The effective media can be described with dynamic effective properties and same imposed $(\omega,\boldsymbol{k})$ dependence.

of periodic arrays of identical inhomogeneities for 1D, 2D, and 3D space in Sec. III E. The procedure may be generalized to random arrays and the point of departure from general arrays to periodic arrays will be highlighted in Sec. III C.

A. Source-driven homogenization theory

Consider a homogeneous fluid characterized by mass density ρ_0 and adiabatic compressibility β_0, which contains an arbitrary, externally controlled source distribution. The acoustic pressure field that results from such a source distribution is shown in Fig. 3(a). The source distribution exists at every point and can be modeled with time-harmonic body forces (dipole sources) with strength $\boldsymbol{f}_{\text{ext}}$ and time-harmonic volume velocity (monopole sources) with strength q_{ext}. The source distribution imposes an arbitrary $e^{i\boldsymbol{k}\cdot\boldsymbol{x}}e^{-i\omega t}$ dependence in the background medium. Although fictitious in practice, a continuous source distribution permits the ability to independently impose acoustic pressure and velocity fields with any desired $(\omega,\boldsymbol{k})$ pair, which makes it possible to uniquely determine the constitutive properties for any $(\omega,\boldsymbol{k})$ combination [4–6] This is the basis of the so-called "source-driven" homogenization approach.

The inhomogeneous linear acoustic equations for conservation of momentum (8) and mass (9) under an $e^{i\boldsymbol{k}\cdot\boldsymbol{x}}e^{-i\omega t}$ driven condition become

$$\begin{aligned} i\boldsymbol{k}\, p_{\text{ext}} &= i\omega\rho_0 \boldsymbol{u}_{\text{ext}} + \boldsymbol{f}_{\text{ext}}, \\ i\boldsymbol{k}\cdot\boldsymbol{u}_{\text{ext}} &= i\omega\beta_0 p_{\text{ext}} + q_{\text{ext}}, \end{aligned} \tag{10}$$

where p_{ext} and $\boldsymbol{u}_{\text{ext}}$ are the complex amplitudes of the acoustic pressure and particle velocity fields, respectively, that result from the externally controlled dipole $\boldsymbol{f}_{\text{ext}}e^{i\boldsymbol{k}\cdot\boldsymbol{x}}$ and monopole $q_{\text{ext}}e^{i\boldsymbol{k}\cdot\boldsymbol{x}}$ source distributions. The space and time dependencies $e^{i\boldsymbol{k}\cdot\boldsymbol{x}}e^{-i\omega t}$ have been suppressed in Eq. (10).

Introducing a random array of small inhomogeneities into the fluid with the same externally controlled source distribution, as illustrated in Fig. 3(b), the conservation equations can be expressed as

$$\begin{aligned} \nabla p(\boldsymbol{x}) &= i\omega\rho_0 \boldsymbol{u}(\boldsymbol{x}) + i\omega \boldsymbol{D}(\boldsymbol{x}) + \boldsymbol{f}_{\text{ext}} e^{i\boldsymbol{k}\cdot\boldsymbol{x}}, \\ \nabla\cdot\boldsymbol{u}(\boldsymbol{x}) &= i\omega\beta_0 p(\boldsymbol{x}) - i\omega M(\boldsymbol{x}) + q_{\text{ext}} e^{i\boldsymbol{k}\cdot\boldsymbol{x}}. \end{aligned} \tag{11}$$

These relationships determine the *microscopic* fields at every point in the medium in terms of the dipole polarization $\boldsymbol{D}(\boldsymbol{x}) = [\rho(\boldsymbol{x}) - \rho_0]\boldsymbol{u}(\boldsymbol{x})$ and monopole polarization $M(\boldsymbol{x}) = -[\beta(\boldsymbol{x}) - \beta_0]p(\boldsymbol{x})$. The polarizations account for the contrast in density and compressibility between the background medium and the inhomogeneities.

Using continuous source distributions to impose an arbitrary $(\omega,\boldsymbol{k})$ pair, one may assume that the effective field amplitudes for a representative unit cell are uniquely determined [4–6] by

$$\begin{aligned} i\boldsymbol{k}\, p_{\text{eff}} &= i\omega\rho_0 \boldsymbol{u}_{\text{eff}} + i\omega \boldsymbol{D}_{\text{eff}} + \boldsymbol{f}_{\text{ext}}, \\ i\boldsymbol{k}\cdot\boldsymbol{u}_{\text{eff}} &= i\omega\beta_0 p_{\text{eff}} - i\omega M_{\text{eff}} + q_{\text{ext}}, \end{aligned} \tag{12}$$

where $\boldsymbol{D}_{\text{eff}}$ and M_{eff} are the effective dipole and monopole polarizations, respectively. This form is guaranteed for periodic arrays. An effective field distribution in the homogenized media is shown in Fig. 3(c), which has the same spatial dependence as the homogeneous background media [Fig. 3(a)], however, the field amplitudes are different, i.e., $p_{\text{ext}} \neq p_{\text{eff}}$, due to the presence of microscale inhomogeneities. By comparing Eq. (12) and the conventional continuity expressions (8) and (9), the constitutive relations relating effective fields in the homogenized medium can be written as

$$\begin{aligned} \boldsymbol{\mu}_{\text{eff}} &= \rho_0 \boldsymbol{u}_{\text{eff}} + \boldsymbol{D}_{\text{eff}}, \\ \varepsilon_{\text{eff}} &= -\beta_0 p_{\text{eff}} + M_{\text{eff}}, \end{aligned} \tag{13}$$

where $\boldsymbol{\mu}_{\text{eff}}$ and ε_{eff} are the effective momentum density and volume strain field amplitudes, respectively. The challenge of determining the effective parameters of the homogenized medium, therefore, lies in relating the polarizations $\boldsymbol{D}_{\text{eff}}$ and M_{eff} to the properties of the inhomogeneities, their distribution in the background fluid, and the effective fields p_{eff} and $\boldsymbol{u}_{\text{eff}}$.

A number of procedures to reduce Eq. (11) to a set of *macroscopic* dynamic equations [Eq. (12)], which describe an effective medium, involve field averaging over a representative unit cell, illustrated by the red box in Fig. 3(b), have been proposed in the literature [1–7,9–11,25,26]. Of particular interest, Alù [5] demonstrated in the analogous case in electromagnetism that a simple volume average removing the dominant Fourier components from Eq. (11) is not sufficient to account for nonlocal effects. Since nonlocal effects are important in determining the effective dynamic properties of metamaterials, a Taylor expansion procedure was developed that does account for nonlocal effects. An important result of this procedure is that it demonstrates explicitly that $\boldsymbol{D}(\boldsymbol{x}) = 0$ does not imply $\boldsymbol{D}_{\text{eff}} = 0$, likewise, $M(\boldsymbol{x}) = 0$ does not imply

$M_{\text{eff}} = 0$. If the analogy holds for acoustic wave phenomena, one would expect, for example, a uniform waveguide lined with array of shunt Helmholtz resonators will result in an effective compressibility *and* density different from the fluid in the waveguide, contrary to what is commonly presented in the literature. This is a result of nonlocal effects, which are demonstrated in the derivation and results that follow in this work. The Taylor expansion method has recently been partially adopted for acoustic systems to demonstrate acoustic bianisotropy [27].

A relation between effective and externally imposed fields is found by subtracting Eq. (10) from Eq. (12) and by solvimg for the effective field amplitudes, which yields

$$\begin{aligned} \boldsymbol{u}_{\text{eff}} &= \boldsymbol{u}_{\text{ext}} + \underline{\boldsymbol{K}}_{\text{d}} \cdot \frac{\boldsymbol{D}_{\text{eff}}}{\rho_0} - \boldsymbol{K}_{\text{c}} \frac{1}{Z_0} \frac{M_{\text{eff}}}{\beta_0}, \\ p_{\text{eff}} &= p_{\text{ext}} + \boldsymbol{K}_{\text{c}} \cdot Z_0 \frac{\boldsymbol{D}_{\text{eff}}}{\rho_0} - K_{\text{m}} \frac{M_{\text{eff}}}{\beta_0}, \end{aligned} \tag{14}$$

where polarization weights (K terms) are defined by

$$\begin{aligned} \underline{\boldsymbol{K}}_{\text{d}} &= \frac{\left(k_0^2 - \boldsymbol{k}\cdot\boldsymbol{k}\right)\underline{\boldsymbol{I}} + \boldsymbol{k}\otimes\boldsymbol{k}}{\boldsymbol{k}\cdot\boldsymbol{k} - k_0^2}, \\ K_{\text{m}} &= \frac{k_0^2}{\boldsymbol{k}\cdot\boldsymbol{k} - k_0^2}, \quad \boldsymbol{K}_{\text{c}} = \frac{k_0\boldsymbol{k}}{\boldsymbol{k}\cdot\boldsymbol{k} - k_0^2}. \end{aligned} \tag{15}$$

Here, $\underline{\boldsymbol{I}}$ is the identity matrix, and $k_0 = \omega\sqrt{\rho_0\beta_0}$ and $Z_0 = \sqrt{\rho_0/\beta_0}$ are the characteristic wave number and impedance of the background medium, respectively.

In Eq. (14), p_{eff} is a function of dipole polarization due to the presence of $\boldsymbol{K}_{\text{c}}$, and $\boldsymbol{u}_{\text{eff}}$ is a function of monopole polarization because of $\boldsymbol{K}_{\text{c}}$. For $\boldsymbol{k} \to 0$, the quasistatic limit, $\underline{\boldsymbol{K}}_{\text{d}} = -\underline{\boldsymbol{I}}$, $K_{\text{m}} = -1$, and $\boldsymbol{K}_{\text{c}} = 0$. Only in this limit, the effective velocity field is proportional to only the dipole polarization, and the effective pressure field is proportional only to the monopole polarization. As pointed out by Alù [5] in electromagnetism, "an inherent form of [*Willis*] *coupling at the unit cell level* stems from weak spatial dispersion effects when $[\boldsymbol{k} \neq 0]$, associated with finite phase velocity across each unit cell." As discussed in Sec. II B, Willis coupling in acoustics is coupling between monopole and dipole motion in the material response, which for metamaterials is the unit cell. Noting that $\boldsymbol{K}_{\text{c}}$ is *odd* in $\boldsymbol{k}$, it will contribute to the macroscopic parameters accounting for odd coupling.

Beginning with the polarization weights in Eq. (14) and throughout the paper, subscript "d" will be used to identify *dipole* quantities that relate dipole response contributions to particle velocity (dipole) fields, subscript "m" will be used to identify *monopole* quantities that relate monopole response contributions to pressure (monopole) fields, and subscript "c" will be used to identify *coupling* quantities that relate monopole response contributions to dipole fields and dipole response contributions to monopole fields.

The analysis above has shown that Willis coupling will exist in acoustics if the coupled polarization weight $\boldsymbol{K}_{\text{c}} \neq 0$, which is due to the nonzero phase across the unit cell. However, neither the composition nor the locations of the inhomogeneities have been investigated. The response and interaction of the inhomogeneities will be considered in the sections that follow in order to derive the effective material parameters of the acoustic metamaterial.

B. Microscale effects: Inhomogeneity response

Beginning with the microscale, inhomogeneities will be assumed (i) to satisfy reciprocity, (ii) to be acoustically small, i.e., $k_0 l \ll 1$, where l is its representative length, and (iii) to be well represented by point dipole $\boldsymbol{d_n}$ and monopole $m_{\boldsymbol{n}}$ moments, i.e., quadrapole and higher-order responses are negligible. The subscript $\boldsymbol{n}$ is a vector identifying a particular inhomogeneity. The dipole moment $\boldsymbol{d_n}$ represents the dipole scattering strength of the $\boldsymbol{n}$th inhomogeneity, and the monopole moment $m_{\boldsymbol{n}}$ represents the monopole scattering strength.

Consider the inhomogeneity located at the origin. The local fields p_{loc} and $\boldsymbol{u}_{\text{loc}}$ are defined as the pressure and velocity fields that would exist at the origin in the absence of the inhomogeneity. The dipole and monopole moments of the inhomogeneity are related to the local fields via polarizabilities, which depend on the composition and geometry of the inhomogeneity. The dipole and monopole moments of this inhomogeneity are given by

$$\begin{aligned} \frac{\boldsymbol{d_0}}{\rho_0} &= \underline{\boldsymbol{\alpha}}_{\text{d}} \cdot \boldsymbol{u}_{\text{loc}} - i\boldsymbol{\alpha}_{\text{c}} \frac{1}{Z_0} p_{\text{loc}}, \\ \frac{m_{\boldsymbol{0}}}{\beta_0} &= -i\boldsymbol{\alpha}_{\text{c}} \cdot Z_0 \boldsymbol{u}_{\text{loc}} - \alpha_{\text{m}} p_{\text{loc}}, \end{aligned} \tag{16}$$

where $\underline{\boldsymbol{\alpha}}_{\text{d}}$ is the dipole polarizability that relates the local particle velocity to the dipole moment, α_{m} is the monopole polarizability that relates the local pressure to the monopole moment, and $\boldsymbol{\alpha}_{\text{c}}$ is the coupled polarizability that relates the local particle velocity to the monopole moment and the local pressure to the dipole moment. The polarizabilities $\underline{\boldsymbol{\alpha}}_{\text{d}}$ and α_{m} represent the pure dipole and monopole responses of the inhomogeneity, respectively. The coupled polarizability $\boldsymbol{\alpha}_{\text{c}}$ is only nonzero when the inhomogeneity has some form of asymmetry (parameter distribution or geometric) and embodies the coupled scattering demonstrated in Fig. 2 and discussed in Sec. II B for an isolated inhomogeneity. The polarizabilities have units of volume and can be determined from the scattering matrix of a single inhomogeneity.

In order to solve for effective material properties, Eq. (16) must be inverted, such that the local fields are expressed as

$$\begin{aligned} \boldsymbol{u}_{\text{loc}} &= \tilde{\underline{\boldsymbol{\alpha}}}_{\text{d}} \cdot \frac{\boldsymbol{d_0}}{\rho_0} - i\tilde{\boldsymbol{\alpha}}_{\text{c}} \frac{1}{Z_0} \frac{m_{\boldsymbol{0}}}{\beta_0}, \\ p_{\text{loc}} &= -i\tilde{\boldsymbol{\alpha}}_{\text{c}} \cdot Z_0 \frac{\boldsymbol{d_0}}{\rho_0} - \tilde{\alpha}_{\text{m}} \frac{m_{\boldsymbol{0}}}{\beta_0}, \end{aligned} \tag{17}$$

where complementary polarizabilities are defined as

$$\begin{aligned} \tilde{\underline{\boldsymbol{\alpha}}}_{\text{d}} &= \underline{\boldsymbol{\alpha}}_{\text{d}}^{-1}[\underline{\boldsymbol{I}} + \boldsymbol{\alpha}_{\text{c}} \otimes \tilde{\boldsymbol{\alpha}}_{\text{c}}], \\ \tilde{\alpha}_{\text{m}} &= \alpha_{\text{m}}^{-1}/\Delta_\alpha, \\ \tilde{\boldsymbol{\alpha}}_{\text{c}} &= \boldsymbol{\alpha}_{\text{c}} \cdot (\alpha_{\text{m}}\underline{\boldsymbol{\alpha}}_{\text{d}})^{-1}/\Delta_\alpha, \end{aligned} \tag{18}$$

and $\Delta_\alpha = 1 - \boldsymbol{\alpha}_{\text{c}} \cdot (\alpha_{\text{m}}\underline{\boldsymbol{\alpha}}_{\text{d}})^{-1} \cdot \boldsymbol{\alpha}_{\text{c}}$. If the inhomogeneity is symmetric, $\tilde{\boldsymbol{\alpha}}_{\text{c}} = \boldsymbol{\alpha}_{\text{c}} = 0$, $\tilde{\underline{\boldsymbol{\alpha}}}_{\text{d}} = \underline{\boldsymbol{\alpha}}_{\text{d}}^{-1}$, and $\tilde{\alpha}_{\text{m}} = \alpha_{\text{m}}^{-1}$, and only in the symmetric case, $\tilde{\underline{\boldsymbol{\alpha}}}_{\text{d}}$ and $\tilde{\alpha}_{\text{m}}$ represent pure dipole and monopole responses, respectively. For $\tilde{\boldsymbol{\alpha}}_{\text{c}} \neq 0$, dipole and

monopole responses are not separable, as indicated by the presence of Δ_α in Eq. (18).

Like the polarizabilities, the components of the complementary polarizabilities $\underline{\tilde{\boldsymbol{\alpha}}}_{\mathrm{d}}$, $\tilde{\alpha}_{\mathrm{m}}$, and $\tilde{\boldsymbol{\alpha}}_{\mathrm{c}}$ are functions of the geometry and the material parameters that make up the inhomogeneities. The complementary polarizabilities are therefore independent of the direction of the imposed wave vector, $\boldsymbol{k}$, and thus *even* in $\boldsymbol{k}$. As one may therefore expect, the sections that follow demonstrate that $\tilde{\boldsymbol{\alpha}}_{\mathrm{c}}$ is directly related to macroscopic even coupling as described in Secs. II A and II B.

C. Mesoscale effects: Multiple scattering

Having defined the monopole and dipole moments of a single inhomogeneity in the previous section, their contributions to the local fields of all other inhomogeneities must be determined in order to accurately represent the response of the entire inhomogeneous medium. This is very difficult in general since the local fields are the result of summations of the scattered fields from all inhomogeneities and the imposed fields p_{ext} and $\boldsymbol{u}_{\mathrm{ext}}$. In order to make it possible to calculate the local fields, inhomogeneities are assumed to be acoustically small ($k_0 l \ll 1$) and spaced sufficiently far apart such that near field scattering effects between inhomogeneities are negligible. For the initial formulation, the locations of the inhomogeneities are arbitrary, but the inhomogeneities are assumed to be identical in composition and orientation with respect to the global coordinate system. The latter assumptions (identical inhomogeneities) allow one to assume that the polarizabilities defined in the previous section are the same for each inhomogeneity. The derivation of the local fields as a function of the imposed and scattered fields up to Eq. (21) is otherwise general and may be specialized to 1D, 2D, or 3D depending on the choice of scalar Green's function $g(\boldsymbol{x}|\boldsymbol{x}_n)$, which is defined in Appendix A. The results of this section will be specialized to periodic lattices in Sec. III D.

For acoustically small inhomogeneities in the presence of an incident acoustic field, the scattered fields at a point $\boldsymbol{x_m}$ due to an inhomogeneity located at $\boldsymbol{x_n}$ may be expressed in terms of the dipole and monopole moments of the $\boldsymbol{n}$th inhomogeneity and modified Green's functions with the following expressions:

$$\begin{aligned} \boldsymbol{u}_{\mathrm{s}}(\boldsymbol{x_m}) &= \underline{\boldsymbol{G}}_{\mathrm{d}}^{\boldsymbol{mn}} \cdot \frac{\boldsymbol{d_n}}{\rho_0} - \boldsymbol{G}_{\mathrm{c}}^{\boldsymbol{mn}} \frac{1}{Z_0} \frac{m_{\boldsymbol{n}}}{\beta_0}, \\ p_{\mathrm{s}}(\boldsymbol{x_m}) &= \boldsymbol{G}_{\mathrm{c}}^{\boldsymbol{mn}} \cdot Z_0 \frac{\boldsymbol{d_n}}{\rho_0} - G_{\mathrm{m}}^{\boldsymbol{mn}} \frac{m_{\boldsymbol{n}}}{\beta_0}. \end{aligned} \tag{19}$$

In Eq. (19), the modified Green's functions are defined in Eq. (20) in terms of the scalar Green's function for a reciprocal background medium $g(\boldsymbol{x}|\boldsymbol{x_n})$:

$$\begin{aligned} \underline{\boldsymbol{G}}_{\mathrm{d}}^{\boldsymbol{mn}} &= -\boldsymbol{\nabla}\boldsymbol{\nabla} g(\boldsymbol{x}|\boldsymbol{x_n})|_{\boldsymbol{x}=\boldsymbol{x_m}} = \underline{\boldsymbol{G}}_{\mathrm{d}}^{\boldsymbol{nm}} = \left(\underline{\boldsymbol{G}}_{\mathrm{d}}^{\boldsymbol{mn}}\right)^{\mathrm{T}}, \\ G_{\mathrm{m}}^{\boldsymbol{mn}} &= k_0^2 g(\boldsymbol{x_m}|\boldsymbol{x_n}) = G_{\mathrm{m}}^{\boldsymbol{nm}}, \\ \boldsymbol{G}_{\mathrm{c}}^{\boldsymbol{mn}} &= -ik_0 \boldsymbol{\nabla} g(\boldsymbol{x}|\boldsymbol{x_n})|_{\boldsymbol{x}=\boldsymbol{x_m}} = -\boldsymbol{G}_{\mathrm{c}}^{\boldsymbol{nm}}. \end{aligned} \tag{20}$$

In the expressions above, the dipole modified Green's tensor $\underline{\boldsymbol{G}}_{\mathrm{d}}^{\boldsymbol{mn}}$ relates the inhomogeneity's dipole moment to the scattered particle velocity; the monopole modified Green's scalar $G_{\mathrm{m}}^{\boldsymbol{mn}}$ relates the inhomogeneity's monopole moment to the scattered pressure; and the coupled modified Green's vector $\boldsymbol{G}_{\mathrm{c}}^{\boldsymbol{mn}}$ relates the inhomogeneity's dipole moment to the scattered pressure and monopole moment to the scattered particle velocity.

The exchange of locations $\boldsymbol{x_n} \leftrightarrow \boldsymbol{x_m}$ represents scattering in the opposite direction. The corresponding changes to the modified Green's functions are expressed in Eq. (20). $\underline{\boldsymbol{G}}_{\mathrm{d}}^{\boldsymbol{mn}}$ and $G_{\mathrm{m}}^{\boldsymbol{mn}}$ are unchanged; however, $\boldsymbol{G}_{\mathrm{c}}^{\boldsymbol{mn}}$ undergoes a sign change due to the gradient operation. The sign change for a corresponding change in scattering direction indicates that this component of mesoscale interaction will be odd in wave vector. It will be shown in the following sections that $\boldsymbol{G}_{\mathrm{c}}^{\boldsymbol{mn}}$ contributes to macroscopic odd coupling.

The local fields may now be determined by the summation of the externally imposed fields and the fields scattered from all other inhomogeneities. It is most straightforward to consider an inhomogeneity located at the origin $\boldsymbol{n} = \boldsymbol{0}$, where the local particle velocity and pressure, $\boldsymbol{u}_{\mathrm{loc}}$ and p_{loc}, may be expressed as

$$\begin{aligned} \boldsymbol{u}_{\mathrm{loc}} &= \boldsymbol{u}_{\mathrm{ext}} + \sum_{\boldsymbol{n}\neq\boldsymbol{0}} \left(\underline{\boldsymbol{G}}_{\mathrm{d}}^{\boldsymbol{0n}} \cdot \frac{\boldsymbol{d_n}}{\rho_0} - \boldsymbol{G}_{\mathrm{c}}^{\boldsymbol{0n}} \frac{1}{Z_0} \frac{m_{\boldsymbol{n}}}{\beta_0} \right), \\ p_{\mathrm{loc}} &= p_{\mathrm{ext}} + \sum_{\boldsymbol{n}\neq\boldsymbol{0}} \left(\boldsymbol{G}_{\mathrm{c}}^{\boldsymbol{0n}} \cdot Z_0 \frac{\boldsymbol{d_n}}{\rho_0} - G_{\mathrm{m}}^{\boldsymbol{0n}} \frac{m_{\boldsymbol{n}}}{\beta_0} \right). \end{aligned} \tag{21}$$

In order to quantify the scattering interaction between unit cells, one must determine the relation between moments of a pair of inhomogeneities, i.e., the relations between the moments of the $\boldsymbol{i}$th and $\boldsymbol{j}$th inhomogeneities: $\boldsymbol{d_i}$ and $\boldsymbol{d_j}$, $\boldsymbol{d_i}$ and m_j, and m_i and m_j. For an arbitrary array, this requires knowledge of the local fields at every inhomogeneity location, which is not possible in general. However, as demonstrated in the next section, the case of periodic arrays results in converging lattice sums, which significantly simplifies the procedure to quantify unit-cell interaction.

D. Periodic array

The existence of an infinite periodic lattice of inhomogeneities significantly reduces the problem of quantifying the interaction between unit cells, and it suffices to proceed with the analysis on a single unit cell, which for simplicity will be centered on the origin. For the case of periodic arrays, the dipole and monopole moments of the $\boldsymbol{n}$th inhomogeneity are directly related to the moments of the inhomogeneity at the origin through application of the Floquet condition: $\boldsymbol{d_n} = \boldsymbol{d_0} e^{i\boldsymbol{k}\cdot\boldsymbol{x_n}}$ and $m_{\boldsymbol{n}} = m_{\boldsymbol{0}} e^{i\boldsymbol{k}\cdot\boldsymbol{x_n}}$. Equation (21) are then given by

$$\begin{aligned} \boldsymbol{u}_{\mathrm{loc}} &= \boldsymbol{u}_{\mathrm{ext}} + \underline{\boldsymbol{C}}_{\mathrm{d}} \cdot \frac{\boldsymbol{d_0}}{\rho_0} - \boldsymbol{C}_{\mathrm{c}} \frac{1}{Z_0} \frac{m_{\boldsymbol{0}}}{\beta_0}, \\ p_{\mathrm{loc}} &= p_{\mathrm{ext}} + \boldsymbol{C}_{\mathrm{c}} \cdot Z_0 \frac{\boldsymbol{d_0}}{\rho_0} - C_{\mathrm{m}} \frac{m_{\boldsymbol{0}}}{\beta_0}, \end{aligned} \tag{22}$$

where the interaction coefficients are defined by

$$\begin{aligned}\underline{\boldsymbol{C}}_{\mathrm{d}} &= \sum_{\boldsymbol{n}\neq 0} e^{i\boldsymbol{k}\cdot\boldsymbol{x}_{\boldsymbol{n}}}\underline{\boldsymbol{G}}_{\mathrm{d}}^{\boldsymbol{0n}},\\ C_{\mathrm{m}} &= \sum_{\boldsymbol{n}\neq 0} e^{i\boldsymbol{k}\cdot\boldsymbol{x}_{\boldsymbol{n}}} G_{\mathrm{m}}^{\boldsymbol{0n}},\\ \boldsymbol{C}_{\mathrm{c}} &= \sum_{\boldsymbol{n}\neq 0} e^{i\boldsymbol{k}\cdot\boldsymbol{x}_{\boldsymbol{n}}}\boldsymbol{G}_{\mathrm{c}}^{\boldsymbol{0n}}.\end{aligned} \tag{23}$$

Each interaction coefficient in Eq. (22) quantifies a different contribution to the local fields from the fields scattered by an infinite periodic array of inhomogeneities. The dipole interaction tensor of coefficients $\underline{\boldsymbol{C}}_{\mathrm{d}}$ quantifies the contributions to the local velocity at the origin related to the dipole moments $\boldsymbol{d}_{\boldsymbol{n}}$ resulting from the local fields at locations $\boldsymbol{x}_{\boldsymbol{n}}$ of all other inhomogeneities. Similarly, the monopole interaction coefficient C_{m} quantifies the contributions to the local pressure at the origin related to the monopole moments $m_{\boldsymbol{n}}$ resulting from the local fields at locations $\boldsymbol{x}_{\boldsymbol{n}}$ of all other inhomogeneities, and the coupled interaction vector of coefficients $\boldsymbol{C}_{\mathrm{c}}$ quantifies the contributions to the local velocity at the origin related to the monopole moments $m_{\boldsymbol{n}}$ and contributions to the local pressure at the origin related to the dipole moments $\boldsymbol{d}_{\boldsymbol{n}}$ resulting from the local fields at locations $\boldsymbol{x}_{\boldsymbol{n}}$ of all other inhomogeneities. It is important to note that these interaction coefficients are purely a function of the modified Green's functions, the periodic spatial distribution of the inhomogeneities, and the imposed wave vector. One can therefore determine these coefficients for any given lattice arrangement assuming that a convergent lattice sum can be found.

The externally imposed field amplitudes may now be expressed in terms of the complementary polarizabilities, interaction coefficients, and dipole and monopole moments by eliminating the local fields in Eqs. (17) and (22) to yield

$$\begin{aligned}\boldsymbol{u}_{\mathrm{ext}} &= (\underline{\tilde{\boldsymbol{\alpha}}}_{\mathrm{d}} - \underline{\boldsymbol{C}}_{\mathrm{d}})\cdot\frac{\boldsymbol{d_0}}{\rho_0} - (i\tilde{\boldsymbol{\alpha}}_{\mathrm{c}} - \boldsymbol{C}_{\mathrm{c}})\frac{1}{Z_0}\frac{m_{\boldsymbol{0}}}{\beta_0},\\ p_{\mathrm{ext}} &= (-i\tilde{\boldsymbol{\alpha}}_{\mathrm{c}} - \boldsymbol{C}_{\mathrm{c}})\cdot Z_0\frac{\boldsymbol{d_0}}{\rho_0} - (\tilde{\alpha}_{\mathrm{m}} - C_{\mathrm{m}})\frac{m_{\boldsymbol{0}}}{\beta_0}.\end{aligned} \tag{24}$$

In the absence of the imposed fields, i.e., $p_{\mathrm{ext}} = 0$ and $\boldsymbol{u}_{\mathrm{ext}} = 0$, Eq. (24) can be rearranged into the following transcendental equation:

$$\begin{aligned}&\det[(\tilde{\alpha}_{\mathrm{m}} - C_{\mathrm{m}})(\underline{\tilde{\boldsymbol{\alpha}}}_{\mathrm{d}} - \underline{\boldsymbol{C}}_{\mathrm{d}})\\ &\quad - (i\tilde{\boldsymbol{\alpha}}_{\mathrm{c}} - \boldsymbol{C}_{\mathrm{c}})\otimes(-i\tilde{\boldsymbol{\alpha}}_{\mathrm{c}} - \boldsymbol{C}_{\mathrm{c}})] = 0.\end{aligned} \tag{25}$$

The solutions to Eq. (25) provide the eigenmodal pairs $(\omega,\boldsymbol{k})$ for any periodic array described by complementary polarizabilities and interaction coefficients. Although this expression is compact, it is important to reiterate that it includes both microscale and mesoscale effects to determine macroscopic eigenmodal pairs. In other words, both the local response of the inhomogeneity and the nonlocal multiple scattering lattice contributions are included in this formulation. Only a few assumptions have been made to achieve the compact representation in Eq. (25): (i) the background medium satisfies reciprocity, and the inhomogeneities (ii) satisify reciprocity, are (iii) acoustically small, (iv) identically oriented, and (v) arranged periodically. Complementary polarizabilities and interaction coefficients are not trivial to find, but the derivation up to this point is exceptionally general.

Although the interaction coefficients contain infinite summations, they all have analytic representations for 1D periodic systems. To the authors' knowledge, rapidly convergent series have been found for C_{m} and $\underline{\boldsymbol{C}}_{\mathrm{d}}$ for 2D and 3D cubic arrays [60], but are yet to be determined for $\boldsymbol{C}_{\mathrm{c}}$ or more general periodic lattices. For simplicity, the results presented here will be restricted to the 1D case, leaving more general cases for future work. It is important to emphasize, however, that the model derived here is completely general for 1D, 2D, and 3D periodic lattices and, therefore, the observations and the physical phenomena they illustrate apply to all cases where inhomogeneities are acoustically small and periodically distributed in a background medium.

E. Effective material parameters

As discussed in Sec. III A and exemplified by the constitutive relations (13), the effective polarizations $\boldsymbol{D}_{\mathrm{eff}}$ and M_{eff} demonstrate how the effective media differ from the background fluid, where $\boldsymbol{D}_{\mathrm{eff}}$ is the additional momentum density and M_{eff} is the additional volume strain of the unit cell. The total response of the inhomogeneity quantifies this additional momentum density and volume strain. It was assumed in Sec. III B that this total response could be represented by monopole and dipole motion [Eq. (16)], which were quantified in terms of the composition and geometry of the inhomogeneity via polarizabilities and the total local field due to externally imposed fields and scattered fields via interaction coefficients. Generally, $\boldsymbol{D}_{\mathrm{eff}}$ is the density of dipole moments in the unit cell, implying $\boldsymbol{D}_{\mathrm{eff}} = \boldsymbol{d_0}/V$; M_{eff} is the density of monopole moments, or $M_{\mathrm{eff}} = m_{\boldsymbol{0}}/V$; and V is the volume of the unit cell.

Combining Eqs. (14) and (24) and eliminating the imposed fields, the effective fields in terms of the polarizations are given by

$$\begin{aligned}\boldsymbol{u}_{\mathrm{eff}} &= \underline{\tilde{\boldsymbol{\Lambda}}}_{\mathrm{d}}\cdot\frac{\boldsymbol{D}_{\mathrm{eff}}}{\rho_0} - \left(\tilde{\boldsymbol{\Lambda}}_{\mathrm{c}}^{\mathrm{o}} + i\tilde{\boldsymbol{\Lambda}}_{\mathrm{c}}^{\mathrm{e}}\right)\frac{1}{Z_0}\frac{M_{\mathrm{eff}}}{\beta_0},\\ p_{\mathrm{eff}} &= \left(\tilde{\boldsymbol{\Lambda}}_{\mathrm{c}}^{\mathrm{o}} - i\tilde{\boldsymbol{\Lambda}}_{\mathrm{c}}^{\mathrm{e}}\right)\cdot Z_0\frac{\boldsymbol{D}_{\mathrm{eff}}}{\rho_0} - \tilde{\Lambda}_{\mathrm{m}}\frac{M_{\mathrm{eff}}}{\beta_0},\end{aligned} \tag{26}$$

where

$$\begin{aligned}\underline{\tilde{\boldsymbol{\Lambda}}}_{\mathrm{d}} &= V\underline{\tilde{\boldsymbol{\alpha}}}_{\mathrm{d}} - V\underline{\boldsymbol{C}}_{\mathrm{d}} + \underline{\boldsymbol{K}}_{\mathrm{d}},\\ \tilde{\Lambda}_{\mathrm{m}} &= V\tilde{\alpha}_{\mathrm{m}} - VC_{\mathrm{m}} + K_{\mathrm{m}},\\ \tilde{\boldsymbol{\Lambda}}_{\mathrm{c}}^{\mathrm{o}} &= -V\boldsymbol{C}_{\mathrm{c}} + \boldsymbol{K}_{\mathrm{c}},\\ \tilde{\boldsymbol{\Lambda}}_{\mathrm{c}}^{\mathrm{e}} &= V\tilde{\boldsymbol{\alpha}}_{\mathrm{c}}.\end{aligned} \tag{27}$$

The tensor $\underline{\tilde{\boldsymbol{\Lambda}}}_{\mathrm{d}}$ only consists of terms relating dipole fields, and the scalar $\tilde{\Lambda}_{\mathrm{m}}$ only consists of terms relating monopole fields. All of the components of $\underline{\tilde{\boldsymbol{\Lambda}}}_{\mathrm{d}}$ and $\tilde{\Lambda}_{\mathrm{m}}$ are even with respect to propagation direction. Noting the signs in front of the two vectors containing coupling terms $\tilde{\boldsymbol{\Lambda}}_{\mathrm{c}}^{\mathrm{o}}$ and $\tilde{\boldsymbol{\Lambda}}_{\mathrm{c}}^{\mathrm{e}}$, in both Eq. (26), one might naturally separate the terms comprising these vectors. However, from the detailed analysis of the preceding sections, the components of $\tilde{\boldsymbol{\Lambda}}_{\mathrm{c}}^{\mathrm{o}}$ are both mesoscale effects and odd with respect to a reversal of propagation,

whereas $\tilde{\boldsymbol{\Lambda}}_{\mathrm{c}}^{\mathrm{e}}$ is due asymmetry at the microscale and even with respect to propagation, as presented in Eq. (27).

To determine effective parameters, Eq. (26) must be inverted, expressing effective polarizations in terms of effective fields as

$$\begin{aligned}\frac{\boldsymbol{D}_{\mathrm{eff}}}{\rho_0} &= \underline{\boldsymbol{\Lambda}}_{\mathrm{d}} \cdot \boldsymbol{u}_{\mathrm{eff}} - \left(\boldsymbol{\Lambda}_{\mathrm{c}}^{\mathrm{o}} + i\boldsymbol{\Lambda}_{\mathrm{c}}^{\mathrm{e}}\right)\frac{1}{Z_0} p_{\mathrm{eff}},\\ \frac{M_{\mathrm{eff}}}{\beta_0} &= \left(\boldsymbol{\Lambda}_{\mathrm{c}}^{\mathrm{o}} - i\boldsymbol{\Lambda}_{\mathrm{c}}^{\mathrm{e}}\right) \cdot Z_0 \boldsymbol{u}_{\mathrm{eff}} - \Lambda_{\mathrm{m}} p_{\mathrm{eff}},\end{aligned} \tag{28}$$

where

$$\begin{aligned}\underline{\boldsymbol{\Lambda}}_{\mathrm{d}} &= \underline{\tilde{\boldsymbol{\Lambda}}}_{\mathrm{d}}^{-1}\left[\underline{\boldsymbol{I}} + \left(\tilde{\boldsymbol{\Lambda}}_{\mathrm{c}}^{\mathrm{o}} + i\tilde{\boldsymbol{\Lambda}}_{\mathrm{c}}^{\mathrm{e}}\right) \otimes \left(\boldsymbol{\Lambda}_{\mathrm{c}}^{\mathrm{o}} - i\boldsymbol{\Lambda}_{\mathrm{c}}^{\mathrm{e}}\right)\right],\\ \Lambda_{\mathrm{m}} &= \tilde{\Lambda}_{\mathrm{m}}^{-1}/\Delta_{\tilde{\Lambda}},\\ \boldsymbol{\Lambda}_{\mathrm{c}}^{\mathrm{o}} &= \tilde{\boldsymbol{\Lambda}}_{\mathrm{c}}^{\mathrm{o}} \cdot (\tilde{\Lambda}_{\mathrm{m}}\underline{\tilde{\boldsymbol{\Lambda}}}_{\mathrm{d}})^{-1}/\Delta_{\tilde{\Lambda}},\\ \boldsymbol{\Lambda}_{\mathrm{c}}^{\mathrm{e}} &= \tilde{\boldsymbol{\Lambda}}_{\mathrm{c}}^{\mathrm{e}} \cdot (\tilde{\Lambda}_{\mathrm{m}}\underline{\tilde{\boldsymbol{\Lambda}}}_{\mathrm{d}})^{-1}/\Delta_{\tilde{\Lambda}},\end{aligned} \tag{29}$$

and $\Delta_{\tilde{\Lambda}} = 1 - (\tilde{\boldsymbol{\Lambda}}_{\mathrm{c}}^{\mathrm{o}} - i\tilde{\boldsymbol{\Lambda}}_{\mathrm{c}}^{\mathrm{e}}) \cdot (\tilde{\Lambda}_{\mathrm{m}}\underline{\tilde{\boldsymbol{\Lambda}}}_{\mathrm{d}})^{-1} \cdot (\tilde{\boldsymbol{\Lambda}}_{\mathrm{c}}^{\mathrm{o}} + i\tilde{\boldsymbol{\Lambda}}_{\mathrm{c}}^{\mathrm{e}})$.

Equations (16) and (28) may be thought of as macro-micro pairs where the macroscopic expression (28) contains information about the microscale and mesoscale physics. Substituting the polarizations provided by Eq. (28) into the constitutive relations (13) yields

$$\begin{aligned}\boldsymbol{\mu}_{\mathrm{eff}} &= \underline{\boldsymbol{\rho}}_{\mathrm{eff}} \cdot \boldsymbol{u}_{\mathrm{eff}} - \left(\boldsymbol{\chi}_{\mathrm{eff}}^{\mathrm{o}} + i\boldsymbol{\chi}_{\mathrm{eff}}^{\mathrm{e}}\right) p_{\mathrm{eff}},\\ \varepsilon_{\mathrm{eff}} &= \left(\boldsymbol{\chi}_{\mathrm{eff}}^{\mathrm{o}} - i\boldsymbol{\chi}_{\mathrm{eff}}^{\mathrm{e}}\right) \cdot \boldsymbol{u}_{\mathrm{eff}} - \beta_{\mathrm{eff}} p_{\mathrm{eff}},\end{aligned} \tag{30}$$

where

$$\begin{aligned}\frac{\underline{\boldsymbol{\rho}}_{\mathrm{eff}}}{\rho_0} &= \underline{\boldsymbol{I}} + \underline{\boldsymbol{\Lambda}}_{\mathrm{d}}, \quad \frac{\beta_{\mathrm{eff}}}{\beta_0} = 1 + \Lambda_{\mathrm{m}},\\ c_0\boldsymbol{\chi}_{\mathrm{eff}}^{\mathrm{o}} &= \boldsymbol{\Lambda}_{\mathrm{c}}^{\mathrm{o}}, \quad c_0\boldsymbol{\chi}_{\mathrm{eff}}^{\mathrm{e}} = \boldsymbol{\Lambda}_{\mathrm{c}}^{\mathrm{e}}.\end{aligned} \tag{31}$$

Equation (30) demonstrates the same coupled form as the bianisotropic relations in electromagnetism [Eq. (1)] and the Willis relations in elastodynamics [Eq. (3)]. The effective density tensor $\underline{\boldsymbol{\rho}}_{\mathrm{eff}}$ relates the effective velocity to the effective momentum; the effective compressibility scalar β_{eff} relates the effective pressure to the effective volume strain; and the odd and even effective coupling vectors $\boldsymbol{\chi}_{\mathrm{eff}}^{\mathrm{o}}$ and $\boldsymbol{\chi}_{\mathrm{eff}}^{\mathrm{e}}$ relate the effective pressure to the effective momentum and the effective velocity to the effective volume strain.

Due to the inversion required to derive Eq. (28), all the effective parameters are, to some order, a function of every microscale response and mesoscale interaction. Although to first order, $\Delta_{\tilde{\Lambda}} \approx 1$, which leads to $\underline{\boldsymbol{\Lambda}}_{\mathrm{d}} \approx \underline{\tilde{\boldsymbol{\Lambda}}}_{\mathrm{d}}^{-1}$, $\Lambda_{\mathrm{m}} \approx \tilde{\Lambda}_{\mathrm{m}}^{-1}$, $\boldsymbol{\Lambda}_{\mathrm{c}}^{\mathrm{o}} \approx \tilde{\boldsymbol{\Lambda}}_{\mathrm{c}}^{\mathrm{o}} \cdot (\tilde{\Lambda}_{\mathrm{m}}\underline{\tilde{\boldsymbol{\Lambda}}}_{\mathrm{d}})^{-1}$, and $\boldsymbol{\Lambda}_{\mathrm{c}}^{\mathrm{e}} \approx \tilde{\boldsymbol{\Lambda}}_{\mathrm{c}}^{\mathrm{e}} \cdot (\tilde{\Lambda}_{\mathrm{m}}\underline{\tilde{\boldsymbol{\Lambda}}}_{\mathrm{d}})^{-1}$. Therefore, in this limit, the effective density is only related to dipole effects; effective compressibility only related to monopole effects; odd coupling is related to mesoscale effects and monopole and dipole effects; and even coupling is related to microscale effects and monopole and dipole effects. As discussed in Sec. III B, a symmetric inhomogeneity results in $\tilde{\boldsymbol{\alpha}}_{\mathrm{c}} = 0$ and, therefore, from Eqs. (27), (29), and (31), $\boldsymbol{\chi}_{\mathrm{eff}}^{\mathrm{e}} = 0$. However, there will still be odd coupling, $\boldsymbol{\chi}_{\mathrm{eff}}^{\mathrm{o}} \neq 0$, due to unit-cell interaction and finite phase speed across the unit cell, which in general may not be neglected. If it is neglected, the calculated effective parameters may lose physical meaning [5,13], which is demonstrated in the following section.

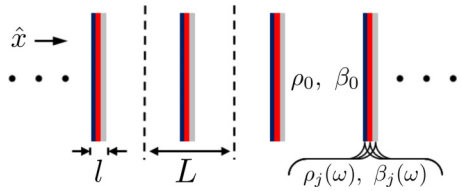

FIG. 4. Schematic of source-free 1D periodic medium with plane-wave propagation along the x axis, period L, background parameters β_0 and ρ_0, total inhomogeneity size l, and inhomogeneity properties $\rho_j(\omega)$ and $\beta_j(\omega)$.

The homogenization procedure presented in this section was quite general, with only a few simplifying assumptions. The polarizabilities of a few canonical geometries are available analytically, and for more complex inhomogeneities, polarizabilities may be calculated from full-wave simulations. Also, the interaction coefficients are available in closed form for only a few periodic lattice geometries. In Sec. IV, exact solutions for polarizabilities and interaction coefficients are obtained for 1D, and examples are considered that demonstrate the utility of the approach and the need to include effective material properties with coupled constitutive relationships.

IV. SOURCE-FREE 1D INSIGHTS

A primary drawback of multiple scattering models is the difficulty in evaluating the polarizabilities introduced in Eq. (16) and the interaction coefficients introduced in Eq. (23). However, for 1D periodic media, these features have exact, closed-form expressions that reveal the odd and even nature of coupling. Additionally, 1D acoustics experiments may be easily developed, simulated, and solved analytically using scalar transmission line techniques, such as transmission and scattering matrices [61]. An example, source-free, 1D periodic medium with period L is depicted in Fig. 4, where longitudinal plane-wave propagation is assumed along the x axis, which is indicated by the unit vector $\hat{x}$. The background media have properties ρ_0 and β_0 and representative cross-sectional area A, and the inhomogeneities are composed of N layers with the jth layer characterized by $\rho_j(\omega)$ and $\beta_j(\omega)$, length l_j, and cross section A_j, where $\sum_{j=1}^{N} l_j = l$. The cross-sectional area A cancels out in the parameter derivation, and the cross section of the inhomogeneity layers is allowed to differ from the background region because changes of cross section are commonly used in acoustic waveguide experiments.

This section proceeds as follows. Section IV A introduces the 1D *effective* parameters based on the derivation of the previous section. In the absence of sources, the macroscopic parameters are nonunique [4–6] and, therefore, Sec. IV B serves to introduce two alternative macroscopic descriptions referred to as *equivalent* and *Bloch*. In Sec. IV C, parameters are numerically calculated for three example periodic media, and the *effective*, *equivalent*, and *Bloch* macroscopic descriptions are presented and discussed in light of the restrictions on macroscopic material parameters, which were introduced in Sec. II C. The results are summarized in Sec. IV D.

A. 1D effective material parameters

The following sections provide insight into *effective* material parameters derived in Sec. III. The even and odd natures of the two coupling parameters stemming from the polarizabilities and interaction coefficients are verified; the specific acoustic impedance and effective wave number are defined in terms of effective parameters; and leading-order terms are derived.

1. Polarizabilities and interaction coefficients

The polarizabilities for a 1D, N-layer inhomogeneity may be exactly determined from the scattering matrix of a single inhomogeneity in the background medium. The derivation is outlined in Appendix B, and the polarizabilities defined in Eq. (16) are given by

$$\begin{aligned}\alpha_{\mathrm{d}} &= \frac{S_{12} - e^{ik_0 l} - (S_{22}+S_{11})/2}{ik_0/A} e^{-ik_0 l},\\ \alpha_{\mathrm{m}} &= \frac{S_{12} - e^{ik_0 l} + (S_{22}+S_{11})/2}{ik_0/A} e^{-ik_0 l},\\ \boldsymbol{\alpha}_{\mathrm{c}} &= \hat{x}\frac{(S_{22}-S_{11})/2}{k_0/A} e^{-ik_0 l} = \hat{x}\alpha_{\mathrm{c}},\end{aligned} \tag{32}$$

where $\hat{x}$ is the unit vector for the propagation axis. There are two important takeaways from Eq. (32). First, because l is finite, the presence of $e^{-ik_0 l}$ demonstrates that polarizabilities map the exact scattered fields from a finite inhomogeneity to its center thereby representing the inhomogeneity as an infinitesimal point scatterer. Representing the finite inhomogeneity as a point introduces a violation of causality for the polarizabilities, which can be corrected [62]; however, this effect is negligible for small inhomogeneities compared to the violations of causality introduced by ignoring even and odd coupling [5]. The analysis of the causality of the polarizabilities is beyond the scope of this work. Second, the expression for $\boldsymbol{\alpha}_{\mathrm{c}}$ explicitly shows that the vector nature of this term is defined by the coordinate system, and that it is even in wave vector. This confirms the statements made in the previous section. Using Eq. (18), the 1D complementary polarizabilities are given by

$$\begin{aligned}\tilde{\alpha}_{\mathrm{d}} &= \alpha_{\mathrm{d}}^{-1}/\left(1-\alpha_{\mathrm{d}}^{-1}\alpha_{\mathrm{m}}^{-1}\alpha_{\mathrm{c}}^{2}\right),\\ \tilde{\alpha}_{\mathrm{m}} &= \alpha_{\mathrm{m}}^{-1}/\left(1-\alpha_{\mathrm{d}}^{-1}\alpha_{\mathrm{m}}^{-1}\alpha_{\mathrm{c}}^{2}\right),\\ \tilde{\boldsymbol{\alpha}}_{\mathrm{c}} &= \hat{x}\alpha_{\mathrm{c}}\alpha_{\mathrm{d}}^{-1}\alpha_{\mathrm{m}}^{-1}/\left(1-\alpha_{\mathrm{d}}^{-1}\alpha_{\mathrm{m}}^{-1}\alpha_{\mathrm{c}}^{2}\right) = \hat{x}\tilde{\alpha}_{\mathrm{c}}.\end{aligned} \tag{33}$$

The interaction coefficients defined in Eq. (23) also may be solved exactly in 1D. If inhomogeneities are located at positions $\boldsymbol{x_n} = \hat{x}nL$, where n is an integer $(-\infty,\infty)$, interaction coefficients (23) reduce to

$$\begin{aligned}C_{\mathrm{d}} = C_{\mathrm{m}} &= \frac{k_0}{2A}\frac{\sin(k_0 L)}{\cos(k_0 L)-\cos(\hat{x}\cdot\boldsymbol{k}L)} - i\frac{k_0}{2A},\\ \boldsymbol{C}_{\mathrm{c}} &= \hat{x}\frac{k_0}{2A}\frac{\sin(\hat{x}\cdot\boldsymbol{k}L)}{\cos(k_0 L)-\cos(\hat{x}\cdot\boldsymbol{k}L)},\end{aligned} \tag{34}$$

as shown in Appendix C. The dependencies on $\boldsymbol{k}L$ in Eq. (34) clearly demonstrate that monopole and dipole interaction coefficients are independent of propagation direction, whereas the coupled interaction coefficient is indeed odd in $\boldsymbol{k}$. Additionally, the expressions for C_{d} and C_{m} are always complex, but $\boldsymbol{C}_{\mathrm{c}}$ is purely real for real k_0 and $\boldsymbol{k}$.

For passive inhomogeneities, $\mathrm{Im}(\tilde{\alpha}_{\mathrm{d}}) \leqslant -k_0/2A$ and $\mathrm{Im}(\tilde{\alpha}_{\mathrm{m}}) \leqslant -k_0/2A$, where equality occurs when the inhomogeneity is lossless and in this case $\mathrm{Im}(\tilde{\alpha}_{\mathrm{c}}) = 0$ (see Appendix D). The factor $-k_0/2A$ in $\mathrm{Im}(\tilde{\alpha}_{\mathrm{d}})$ and $\mathrm{Im}(\tilde{\alpha}_{\mathrm{m}})$ represents the reradiation from the inhomogeneity, and for lossless inhomogeneities in a periodic array, this term cancels the identical term in the interaction coefficients due to coherent scattering in Eq. (24). In fact, the imaginary parts of the complementary polarizabilities and interaction coefficients cancel for any lossless periodic media in 1D, 2D, or 3D. For nonperiodic inhomogeneous media, the imaginary parts will not cancel and scattering losses [57] will be present in effective parameters, even if all constituents are lossless.

2. Wave number and impedance

For periodic media in the absence of sources, the $(\omega,\boldsymbol{k})$ solutions are the eigenvalues of Eq. (25), and for 1D, $\boldsymbol{k} = \hat{x}k$, where k is the Bloch wave number of the array. Suppressing the unit vector $\hat{x}$, the constitutive relations for 1D become

$$\begin{aligned}\mu_{\mathrm{eff}} &= \rho_{\mathrm{eff}}u_{\mathrm{eff}} - \left(\chi^{\mathrm{o}}_{\mathrm{eff}} + i\chi^{\mathrm{e}}_{\mathrm{eff}}\right)p_{\mathrm{eff}},\\ \varepsilon_{\mathrm{eff}} &= \left(\chi^{\mathrm{o}}_{\mathrm{eff}} - i\chi^{\mathrm{e}}_{\mathrm{eff}}\right)u_{\mathrm{eff}} - \beta_{\mathrm{eff}}p_{\mathrm{eff}}.\end{aligned} \tag{35}$$

The relation between the effective parameters and the wave number may be determined from the conservation equations (8) and (9), which leads to

$$\left(k/\omega + \chi^{\mathrm{o}}_{\mathrm{eff}}\right)^2 = \rho_{\mathrm{eff}}\beta_{\mathrm{eff}} - \left(\chi^{\mathrm{e}}_{\mathrm{eff}}\right)^2 \tag{36}$$

in the absence of sources and, therefore,

$$k^{\pm}/\omega = \pm\sqrt{\rho_{\mathrm{eff}}\beta_{\mathrm{eff}} - \left(\chi^{\mathrm{e}}_{\mathrm{eff}}\right)^2} - \chi^{\mathrm{o}\pm}_{\mathrm{eff}}, \tag{37}$$

where $\pm$ correspond to waves traveling in $\pm\hat{x}$ directions. Notice that for the representation of constitutive relations in Eq. (35), the wave number is a function of all effective parameters (this is not the case for other forms of the constitutive relations, e.g., Refs. [7,14,50]), and odd coupling is direction dependent.

The specific acoustic impedance, derived from the conservation of momentum, may be expressed as

$$\begin{aligned}Z^{\pm} = \frac{p_{\mathrm{eff}}}{u_{\mathrm{eff}}} &= \frac{\rho_{\mathrm{eff}}}{\left(k/\omega + \chi^{\mathrm{o}}_{\mathrm{eff}}\right) + i\chi^{\mathrm{e}}_{\mathrm{eff}}}\\ &= \pm\sqrt{\frac{\rho_{\mathrm{eff}}}{\beta_{\mathrm{eff}}} - \left(\frac{\chi^{\mathrm{e}}_{\mathrm{eff}}}{\beta_{\mathrm{eff}}}\right)^2} - i\frac{\chi^{\mathrm{e}}_{\mathrm{eff}}}{\beta_{\mathrm{eff}}},\end{aligned} \tag{38}$$

which for a passive medium must satisfy $\mathrm{Re}(Z^{+}) \geqslant 0$ and $\mathrm{Re}(Z^{-}) \leqslant 0$. Surprisingly, Eq. (38) indicates that if even coupling exists, the impedance will be complex, even if the medium is lossless, and that the phase angle changes with direction, all of which is not intuitive. However, periodic media with asymmetric unit cells are known to have complex *Bloch* impedances [63], which will be discussed in more detail in Sec. IV B, and it has previously been demonstrated that the specific acoustic impedance must always be complex in Willis materials with even coupling [27,50,64]. The complex nature of the impedance make Willis materials with even coupling ideal for impedance-matching applications, as demonstrated

by Koo *et al.* [27]. Additionally, Eqs. (37) and (38) demonstrate that one cannot determine density and compressibility from only impedance and wave number when there exists nonzero coupling, i.e., $\rho_{\text{eff}} \neq Z^{\pm}k^{\pm}/\omega$ and $\beta_{\text{eff}} \neq k^{\pm}/\omega Z^{\pm}$, which is counter to general assumptions in reflection/transmission acoustical parameter extraction methods [65].

3. Leading-order terms

At this point, it is informative to provide some insight into the relationships between the *effective* material parameters and the volume-averaged parameters, which are often used to estimate the overall response of an inhomogeneous medium. Specifically, it is of interest to understand how the coupling terms relate to the volume-averaged density and compressibility to demonstrate that these terms may not be negligible in the long-wavelength limit. Leading-order terms for the quasistatic limit $k_0 L \to 0$ and $kL \to 0$ were determined for the *effective* material parameters from Taylor expansions of polarizabilities and interaction coefficients. In this limit, the jth material of a multimaterial inhomogeneity may be described by the lumped acoustic mass $M_j^{\text{A}} = \rho_j l_j / A_j$ and acoustic compliance $C_j^{\text{A}} = \beta_j l_j A_j$. For this case, leading-order terms of the effective parameters in terms of acoustic mass and compliance are

$$\begin{aligned}
\rho_{\text{eff}}/\rho_0 &\to 1 - l/L + \sum_{j=1}^{N} \frac{M_j^{\text{A}}}{M_0^{\text{A}}} = \frac{\langle \rho \rangle}{\rho_0}, \\
\beta_{\text{eff}}/\beta_0 &\to 1 - l/L + \sum_{j=1}^{N} \frac{C_j^{\text{A}}}{C_0^{\text{A}}} = \frac{\langle \beta \rangle}{\beta_0}, \\
c_0 \chi_{\text{eff}}^{\text{e}} &\to \frac{k_0 L}{2} \sum_{i=1}^{N-1} \sum_{j=i+1}^{N} \frac{M_i^{\text{A}} C_j^{\text{A}} - M_j^{\text{A}} C_i^{\text{A}}}{M_0^{\text{A}} C_0^{\text{A}}}, \\
c_0 \chi_{\text{eff}}^{\text{o}} &\to \frac{(k_0 L)(kL)}{12} \left(\frac{\langle \rho \rangle}{\rho_0} - 1 \right) \left(\frac{\langle \beta \rangle}{\beta_0} - 1 \right),
\end{aligned} \tag{39}$$

where $M_0^{\text{A}} = \rho_0 L/A$ and $C_0^{\text{A}} = \beta_0 L A$ are the acoustic mass and compliance of the unit cell in the absence of the inhomogeneity, i.e., a volume $V = LA$ of the background media. As might be expected, the *effective* density and compressibility are constants in the quasistatic limit given by their volume-averaged quantities. However, the leading terms of the coupling parameters are not constants. Even coupling is proportional to frequency, $k_0 L = \omega \sqrt{\rho_0 \beta_0} L$, and odd coupling is proportional to frequency multiplied by the macroscopic wave number, $(k_0 L)(kL)$. Because $\chi_{\text{eff}}^{\text{o}}$ provides a metric of the influence of nonlocal effects on the effective response, when the product $(k_0 L)(kL)$ is small, nonlocal effects are likely to be negligible. In Sec. IV C, the examples presented suggest that for $(k_0 L)(kL) < 0.1$ nonlocal effects are negligible. The leading terms in Eq. (39) verify that odd and even coupling are indeed higher-order effects.

Additionally, the frequency dependence of even coupling suggests that time derivative $-i\omega$ has been absorbed into $\chi_{\text{eff}}^{\text{e}}$, due to the way the constitutive relations are expressed in Eq. (35). Nassar *et al.* [26] and Muhlestein *et al.* [14] noticed similar results and suggested that modified constitutive relations would be more meaningful for time-domain studies. Additionally, the frequency and wave-number dependence of odd coupling suggests that both time and spatial derivatives have been absorbed into $\chi_{\text{eff}}^{\text{o}}$. As suggested by Muhlestein *et al.* [14], causality would suggest that parameters be constant in the quasistatic limit. Thus, a more meaningful form of the constitutive relations for time-domain study may be

$$\begin{aligned}
\boldsymbol{\mu}_{\text{eff}} &= \underline{\boldsymbol{\rho}}_{\text{eff}} \cdot \boldsymbol{u}_{\text{eff}} - (\underline{\boldsymbol{\phi}}_{\text{eff}} \cdot \nabla \dot{p}_{\text{eff}} - \boldsymbol{\theta}_{\text{eff}} \dot{p}_{\text{eff}}), \\
\varepsilon_{\text{eff}} &= (\underline{\boldsymbol{\phi}}_{\text{eff}} : \nabla \dot{\boldsymbol{u}}_{\text{eff}} + \boldsymbol{\theta}_{\text{eff}} \cdot \dot{\boldsymbol{u}}_{\text{eff}}) - \beta_{\text{eff}} p_{\text{eff}},
\end{aligned} \tag{40}$$

which are related to the previously defined coefficients by $\boldsymbol{\chi}_{\text{eff}}^{\text{e}} = \omega \boldsymbol{\theta}_{\text{eff}}$ and $\boldsymbol{\chi}_{\text{eff}}^{\text{o}} = \omega \underline{\boldsymbol{\phi}}_{\text{eff}} \cdot \boldsymbol{k}$, and $\boldsymbol{\theta}_{\text{eff}}$ and $\underline{\boldsymbol{\phi}}_{\text{eff}}$ are both even functions in wave number and constant in the quasistatic limit. Often in the frequency domain, the form of the constitutive relations is chosen out of convenience. For this work, constitutive relations were expressed in terms of p and $\boldsymbol{u}$ because these variables are most commonly used in acoustics, and this form is analogous to the $E - H$ convention in electromagnetism [36].

B. Alternative macroscopic descriptions

In the absence of sources, the constitutive relations are nonunique, allowing for alternative macroscopic descriptions. The following sections provide a description that relates effective fields but neglects coupling, referred to as *equivalent* parameters, and a description related to the microscopic fields, referred to as *Bloch* parameters.

1. Equivalent parameters

The constitutive relations for *equivalent* parameters have the same form as a traditional homogeneous fluid (as briefly introduced in Sec. II C), i.e.,

$$\mu_{\text{eff}} = \rho_{\text{eq}} u_{\text{eff}}, \quad \varepsilon_{\text{eff}} = -\beta_{\text{eq}} p_{\text{eff}}, \tag{41}$$

and, correspondingly,

$$k^{\pm}/\omega = \pm \sqrt{\rho_{\text{eq}}^{\pm} \beta_{\text{eq}}^{\pm}}, \tag{42}$$

$$Z^{\pm} = \pm \sqrt{\rho_{\text{eq}}^{\pm} / \beta_{\text{eq}}^{\pm}}. \tag{43}$$

As indicated, the *equivalent* parameters are directionally dependent. This can be seen more clearly by considering the relation between *effective* and *equivalent* parameters, which by using Eqs. (35) and (41) and the conservation equations leads to

$$\begin{aligned}
\rho_{\text{eq}}^{\pm} &= \rho_{\text{eff}} \left(1 + \frac{\chi_{\text{eff}}^{\text{o}\pm} + i \chi_{\text{eff}}^{\text{e}}}{k^{\pm}/\omega} \right)^{-1} = Z^{\pm} k^{\pm}/\omega, \\
\beta_{\text{eq}}^{\pm} &= \beta_{\text{eff}} \left(1 + \frac{\chi_{\text{eff}}^{\text{o}\pm} - i \chi_{\text{eff}}^{\text{e}}}{k^{\pm}/\omega} \right)^{-1} = k^{\pm}/\omega Z^{\pm}.
\end{aligned} \tag{44}$$

Equation (44) provides several insights. First, *equivalent* parameters are determined directly from wave number and impedance. Second, in the absence of even coupling, *equivalent* density and compressibility are not directionally dependent but still differ from the *effective* properties due to finite odd coupling. However, for nonzero even coupling, both *equivalent* density and compressibility will be directionally dependent and complex even for lossless media, in which case the imaginary part of one will be greater than zero (normally

indicative of loss) and the imaginary part of the other will be less than zero (normally indicative of gain) depending on the sign of χ^{e}_{eff} in Eq. (44).

These observations suggest that, while *equivalent* parameters provide knowledge of wave propagation by their relation to impedance and wave number, the *equivalent* parameters themselves lack physical meaning by violating passivity and possibly causality (Sec. II C).

2. *Bloch parameters*

Transmission line analogs have been widely used in the development and understanding of 1D periodic acoustic metamaterials, e.g., Refs. [64,66,67]. Because they maintain the microscopic fields at the boundary of a defined unit cell [64], transmission line models lend themselves well to measurement via the reflection/transmission method popularized by Fokin *et al.* [65], which was recently extended to account for asymmetry [27,50]. However, homogenization schemes, such as those developed in Sec. III, determine effective fields that do not equal microscopic fields at any point in general. Therefore, the parameters determined using transmission line techniques and reflection/transmission measurements are not *effective* or *equivalent* parameters, as defined in this work, but are *Bloch* parameters relating the fields at the boundary of a unit cell defined by a transmission matrix [64] or measurement sample [50,65]. As *Bloch* parameters do not relate effective fields but instead microscopic fields at a point, they cannot account for nonlocal effects, and will not generally satisfy restrictions based on causality [Eq. (7)] [12].

It was demonstrated in the classic work by Brillouin [63] that the *Bloch* impedance changes with position, and if the position results in an asymmetric unit cell, it will be complex. In 1D periodic acoustic media, the microscopic field patterns due to time-harmonic waves are *Bloch* waves [63]. This was demonstrated in 1D periodic acoustic media by Bradley both theoretically [68] and experimentally [69]. Therefore, one may express the *Bloch* impedance, which is the ratio of the microscopic pressure and particle velocity at a point, as [12,63,64]

$$Z^{\pm}_{B(x)} = \frac{p(x)}{u(x)} = \pm\sqrt{\frac{\rho_{B(x)}}{\beta_{B(x)}} - \left(\frac{\chi^{e}_{B(x)}}{\beta_{B(x)}}\right)^{2}} - i\frac{\chi^{e}_{B(x)}}{\beta_{B(x)}}. \quad (45)$$

In periodic media, the *Bloch* wave number is the solution to the transcendental equation (25), and is related to *Bloch* parameters via

$$k^{\pm}/\omega = \pm\sqrt{\rho_{B(x)}\beta_{B(x)} - \left(\chi^{e}_{B(x)}\right)^{2}}. \quad (46)$$

In summary, unlike *effective* and *equivalent* properties, *Bloch* properties (i) only exist for periodic media and (ii) relate the microscopic fields at a point rather than effective fields. While it is convenient for measurements to relate parameters to boundary fields, such an approach does not necessarily lead to physically meaningful parameters that satisfy passivity and causality, as is demonstrated in the following section.

C. Numerical examples

This section presents three 1D periodic media examples without embedded sources. Therefore, macroscopic parameters are nonunique, and wave numbers are the eigenvalues

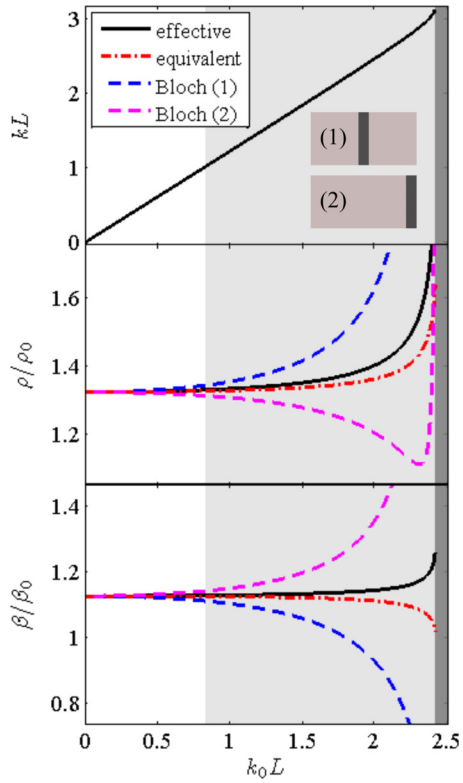

FIG. 5. Normalized macroscopic wave number (top), mass density (middle), and compressibility (bottom) plotted versus normalized frequency for a 1D periodic medium with lead inhomogeneities in an aluminum background, and $l/L = 0.1$. Two different unit cells were used to determine *Bloch* parameters: Bloch (1) corresponds to the inhomogeneity being centered in the unit cell, and Bloch (2) corresponds to the inhomogeneity at the unit-cell boundary, as depicted in the inset of the top panel.

of the lattice, which may be determined from Eq. (25) or using transmission matrices [61]. Under these conditions, the *effective* material parameters (Sec. IV A) may be directly compared to the alternative descriptions (Sec. IV B) referred to as *equivalent* material parameters, which relate effective fields but neglect coupling, and *Bloch* material parameters, which relate microscopic fields at a particular point that define a specific unit cell and cannot account for nonlocal effects. The solutions are presented for longitudinal plane-wave propagation normal to the layers, in the $\hat{x}$ direction, as indicated in Fig. 4. For this case, transverse-to-longitudinal field coupling elastic wave motion may be neglected, and the longitudinal elastic wave behavior can be described by a plane-wave compliance $\beta_{PW} = (\rho c_L^2)^{-1}$, which is consistent with the acoustic analysis of this work. Therefore, the 1D homogenization derived in Sec. IV A can be used to compare with the results of Refs. [7,25].

Figures 5–8, 10, and 11 present normalized macroscopic material parameters plotted versus normalized frequency, $k_0 L = \omega\sqrt{\rho_0\beta_0}L$, and obtained using the *effective* (solid lines), *equivalent* (dashed-dotted lines), and *Bloch* (dashed lines) models for forward propagation in the $+\hat{\boldsymbol{x}}$ direction. In all of these figures, the background shading highlights frequency ranges of interest: (i) white for $|\mathrm{Re}(kL)| < 1$

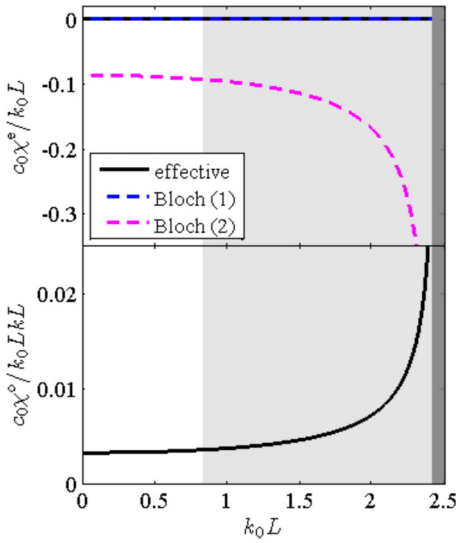

FIG. 6. Normalized macroscopic coupling, even (top) and odd (bottom), plotted versus normalized frequency for a 1D periodic medium with lead inhomogeneities in an aluminum background, and $l/L = 0.1$.

corresponding to wave numbers for which dynamic homogenization is generally accepted [12]; (ii) light gray for $1 \leqslant \mathrm{Re}(kL) < \pi$ corresponding to wave numbers that some suggest [26,70] are reasonable to apply dynamic homogenization; and (iii) dark gray corresponding to stop bands. Unless otherwise noted, material properties were obtained from Appendix A of Ref. [55], and material compressibility was calculated using $\beta = 1/\rho c^2$. The results are discussed in light of the physical restrictions introduced in Sec. II C.

1. Lead inhomogeneities in aluminum

The first example was a two-phase composite consisting of lead inhomogeneities ($\rho_{\mathrm{Pb}} = 11\,300$ kg/m^3, $c_{\mathrm{Pb}} = 2050$ m/s) embedded in aluminum ($\rho_{\mathrm{Al}} = 2700$ kg/m^3, $c_{\mathrm{Al}} = 6300$ m/s) with filling fraction $l/L = 0.1$. Additionally, both lead and aluminum are assumed lossless; therefore, in propagating bands, all macroscopic material parameters should be purely real.

Figure 5 presents the normalized wave number (top), density (middle), and compressibility (bottom). Two unit-cell configurations were used to calculate *Bloch* parameters, which were depicted in the inset in the top panel of Fig. 5. Configuration (1) corresponded to the inhomogeneity being centered in the unit cell, and configuration (2) corresponded to an asymmetric cell configuration with the inhomogeneity on the right. As suggested in Sec. IV A, the dependence of odd coupling on the product $(k_0L)(kL)$ suggests that when this product is small, nonlocal effects may be neglected. For the present example, the macroscopic density and compressibility for the four models converged to volume-averaged quantities for $k_0L < 0.3$, which approximately corresponds to $(k_0L)(kL) < 0.1$, but the models diverge for $k_0L > 0.3$ due to the influence of nonlocal effects. Additionally, negative slopes were observed in the density computed using the *Bloch* (2) model and in the compressibility computed using the *equivalent* and *Bloch* (1) models, even in the quasistatic limit.

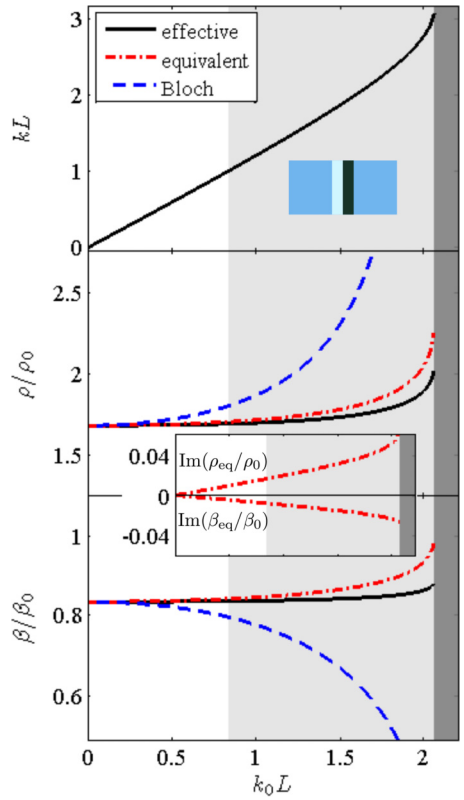

FIG. 7. Normalized macroscopic wave number (top), mass density (middle), and compressibility (bottom) plotted versus normalized frequency for a 1D periodic medium with inhomogeneities consisting of equal parts steel and rubber in an aqueous background, and $l/L = 0.2$. The *Bloch* parameters correspond to the inhomogeneity being centered in the unit cell, as depicted in the inset of the top panel. Additionally, the inset between the middle and bottom panels presents the normalized imaginary parts of the *equivalent* density and compressibility. The presence of even coupling results in complex ρ_{eq} and β_{eq} despite the composite being lossless.

Therefore, only the *effective* model satisfied causality for this medium, as defined in Eq. (7).

Normalized even and odd coupling are presented in the top and bottom panels of Fig. 6, respectively. Because the presence of asymmetry in a two-phase medium is a feature of a particularly defined unit cell, $\chi^{\mathrm{e}} = 0$ for the *effective* and *Bloch* (1) models but is finite for the *Bloch* (2) model. Only the *effective* model can account for nonlocal effects, and even though $\chi^{\mathrm{o}}_{\mathrm{eff}}$ is small, it is nonzero and grows rapidly for $k_0L > 2$.

2. Steel and rubber inhomogeneities in water

The second example was a three-phase composite consisting of steel ($\rho_{\mathrm{st}} = 7700$ kg/m^3, $c_{\mathrm{st}} = 6100$ m/s) and rubber ($\rho_{\mathrm{ru}} = 1100$ kg/m^3, $c_{\mathrm{ru}} = 2400$ m/s) inhomogeneities embedded in water ($\rho_{\mathrm{w}} = 998$ kg/m^3, $c_{\mathrm{w}} = 1481$ m/s), where all materials were assumed to be lossless. The inhomogeneities consisted of equal parts steel and rubber, i.e., $l_{\mathrm{st}} = l_{\mathrm{ru}}$, and the total size of the inhomogeneities, $l = l_{\mathrm{st}} + l_{\mathrm{ru}}$, was varied from $l/L = 0.01$ to 0.5. A 1D three-phase composite always has an asymmetric unit cell regardless of where the unit cell is drawn and, therefore, even coupling should be observed.

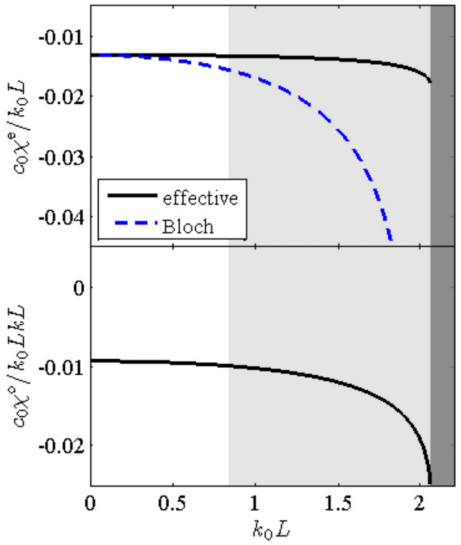

FIG. 8. Normalized macroscopic even coupling (top) and odd coupling (bottom) plotted versus normalized frequency for a 1D periodic medium with inhomogeneities consisting of equal parts steel and rubber in an aqueous background, and $l/L = 0.2$.

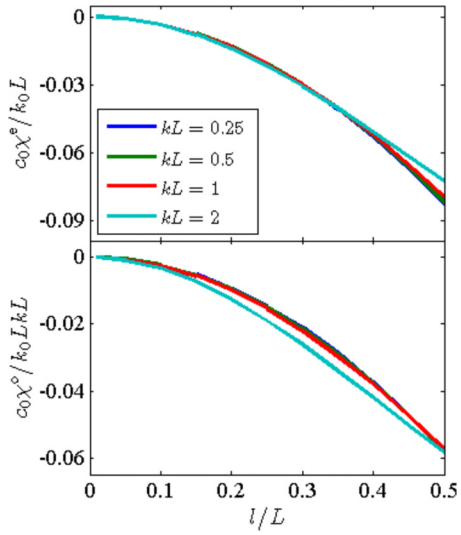

FIG. 9. Normalized *effective* even coupling (top) and odd coupling (bottom) plotted versus inhomogeneity size for a 1D periodic medium with inhomogeneities consisting of equal parts steel and rubber in an aqueous background. Different colored lines correspond to coupling calculated for different wave numbers: $kL = 0.25, 0.5, 1, 2$.

The normalized wave number (top), density (middle), and compressibility (bottom) for $l/L = 0.2$ are presented in Fig. 7, and the *Bloch* parameters were calculated with inhomogeneity centered in the unit cell as depicted in the inset in the top panel. Similar to the first example, the product $(k_0L)(kL) < 0.1$ approximately corresponded to $k_0L < 0.3$ and, again, the models converged on the same values for the macroscopic density and compressibility and diverged for $k_0L > 0.3$ due to odd coupling from nonlocal effects. The only apparent causality violation, denoted by a negative slope, occurred in the compressibility calculated using the *Bloch* model.

Because the *equivalent* model does not account for even coupling, it appears through complex parameters, which is counter to the fact that the composite is lossless. The inset between the middle and bottom panels of Fig. 7 demonstrates that the imaginary parts of *equivalent* density and compressibility are nonzero. Additionally, $\mathrm{Im}(\beta_{\mathrm{eq}}) < 0$ which violates passivity, as shown in Eq. (6), but the combination of *equivalent* density and compressibility result in passive k and Z, as discussed in Sec. II C. Again, only the *effective* density and compressibility satisfy causality and passivity for this composite.

Figure 8 presents normalized even (top) and odd (bottom) coupling plotted versus normalized frequency. The *Bloch* even coupling determined from the unit cell centered on the inhomogeneity matches the *effective* even coupling in the quasistatic limit but diverges for $k_0L > 0.3$ similar to density and compressibility. Again, $\chi^{\mathrm{o}}_{\mathrm{eff}}$ is small, but nonzero, and grows rapidly for $k_0L > 1.5$.

Figure 9 presents normalized *effective* even (top) and odd (bottom) coupling plotted versus volume fraction l/L for several wave numbers. Both coupling parameters increase in magnitude as $(l/L)^2$, and normalized forms are relatively constant for $kL \leqslant 1$, suggesting that the limits for $\chi^{\mathrm{e}}_{\mathrm{eff}}$ and $\chi^{\mathrm{o}}_{\mathrm{eff}}$ in Eq. (39) may be valid for $kL \leqslant 1$. To be consistent in this range, one must also consider second-order effects $(k_0L)^2$ and $(kL)^2$ in ρ_{eff} and β_{eff}, which are not included in the expressions in Eq. (39).

3. *Double-negative inhomogeneities in air*

Lastly, a four-phase composite exhibiting a double-negative frequency band was considered and modeled such that it could be implemented with a rigid-walled waveguide with Helmholtz resonators in shunt and flexible plates in series, similar to the study by Seo *et al.* [67]. The inhomogeneities consisted of three layers: (i) a region with dynamic compressibility, which modeled a Helmholtz resonator in shunt, (ii) a segment of air-filled waveguide, and (iii) a region with dynamic density, which modeled a flexible plate in series with the waveguide.

A Helmholtz resonator in shunt can be modeled as a region with dynamic compressibility [71] with properties defined by $\rho_{\mathrm{H}} = \rho_{\mathrm{air}}, l_{\mathrm{H}}/L = 0.075$, and $\beta_{\mathrm{H}} = \beta_0 v_{\mathrm{H}}/[1 - i\omega_{\mathrm{H}}/(\omega Q_{\mathrm{H}}) - \omega^2/\omega^2_{\mathrm{H}}]$, where $v_{\mathrm{H}} = 10$, $\omega_{\mathrm{H}}L/c_0 = 0.25$, and $Q_{\mathrm{H}} = 20$. The waveguide segment was modeled as air filled ($\rho_{\mathrm{air}} = 1.21\ \mathrm{kg/m^3}$, $c_{\mathrm{air}} = 343\ \mathrm{m/s}$) and $l_{\mathrm{air}}/L = 0.173$. The dynamic density region modeled a Kapton® plate [66] with $1/\beta_{\mathrm{pl}} = E/[3(1-\nu)] = 1.3929\ \mathrm{GPa}$, $l_{\mathrm{pl}}/L = 0.002$, and $\rho_{\mathrm{pl}} = \rho_{\mathrm{k}}[1 + i\omega_{\mathrm{pl}}/(\omega Q_{\mathrm{pl}}) - \omega^2_{\mathrm{pl}}/\omega^2]$, where $\rho_{\mathrm{k}} = 1420\ \mathrm{kg/m^3}$, $\omega_{\mathrm{pl}}L/c_0 = 0.5$, and $Q_{\mathrm{pl}} = 80$. The total relative size of the inhomogeneity was $l/L = 0.25$, where $l = l_{\mathrm{H}} + l_{\mathrm{air}} + l_{\mathrm{pl}}$.

The normalized wave number (top), density (middle), and compressibility (bottom) are presented in Fig. 10, and *Bloch* parameters were calculated with the inhomogeneity centered in the unit cell as depicted in the inset in the top panel. Two passbands existed for this example: a double-negative passband for $0.258 < k_0L < 0.334$, and a double-positive passband for $k_0L > 0.419$. The inequality $(k_0L)|\mathrm{Re}(kL)| < 0.1$ was satisfied in passband portions of the frequency range $0.3 < k_0L < 0.45$. Again, it is near these bounds that the *Bloch* model diverges from the *effective* model for both density and compressibility. Additionally, as observed in the middle panel

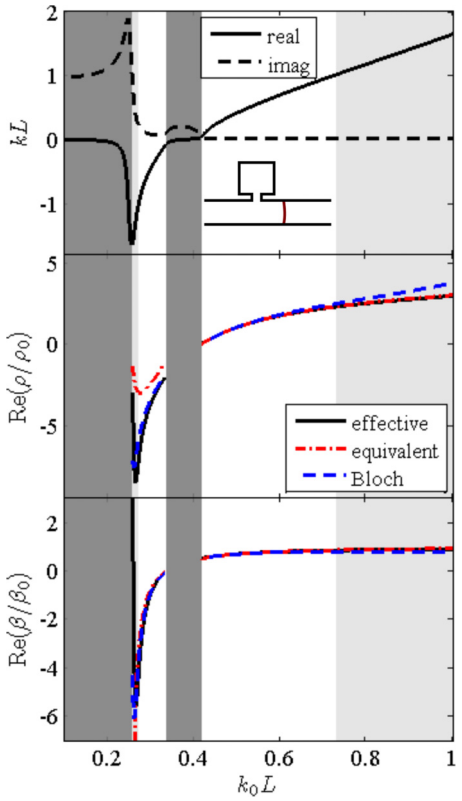

FIG. 10. Normalized macroscopic wave number (top), mass density (middle), and compressibility (bottom) plotted versus normalized frequency for a 1D periodic medium with inhomogeneities consisting of a Helmholtz resonator in shunt, a section of waveguide, and a flexible plate in series in an air background, and $l/L = 0.25$. The *Bloch* parameters correspond to the inhomogeneity being centered in the unit cell, as depicted in the inset of the top panel.

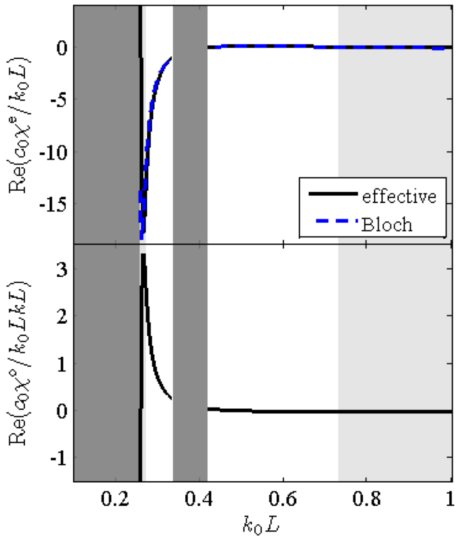

FIG. 11. Normalized macroscopic even coupling (top) and odd coupling (bottom) plotted versus normalized frequency for a 1D periodic medium with inhomogeneities consisting of a Helmholtz resonator in shunt, a section of waveguide, and a flexible plate plate in series in an air background, and $l/L = 0.25$.

of Fig. 10, the *equivalent* density differed from the *Bloch* and *effective* densities in the double-negative band even for small wave numbers. This was not the case in the double-positive band $k_0L > 0.419$, and might suggest that in highly dynamic bands, which inevitably include double-negative bands, even and odd coupling are not negligible.

That even and odd coupling are not negligible is confirmed in Fig. 11. In the double-negative band, both coupling terms significantly exceed values observed in the previous two examples. Again, the *Bloch* even coupling determined from the unit cell centered on the inhomogeneity matches the *effective* even coupling for $k_0L|\mathrm{Re}(kL)| < 0.1$.

D. Summary of 1D examples

Three macroscopic descriptions of 1D periodic media were considered: (i) *effective* parameters which were derived in Sec. III, relate macroscopic effective fields, and account for Willis coupling due to microscopic asymmetry and mesoscale effects, (ii) *equivalent* parameters which relate macroscopic effective fields but neglect coupling and exist due to nonuniqueness in the absence of sources, and (iii) *Bloch* parameters which relate microscopic Bloch fields at a point in periodic media. The comparison of *effective* parameters to *equivalent* and *Bloch* parameters was important because it is often assumed that metamaterials may be described by the same parameters as homogeneous media leading to *equivalent* parameters, and parameters are often determined by reflection/transmission from a single unit cell or transmission matrices, which result in *Bloch* parameters [12].

For symmetric examples near the quasistatic limit, all three macroscopic descriptions provided similar results, as shown in Fig. 5, and for asymmetric examples, *Bloch* parameters converged to *effective* parameters when nonlocal effects are negligible, i.e., $(k_0L)|\mathrm{Re}(kL)| < 0.1$, as shown in Figs. 7, 8, 10, and 11. Within these limits, reflection/transmission measurements of a single unit cell will lead to meaningful parameters of an infinite periodic medium consisting of the unit cell measured, if the inhomogeneity is centered in the unit cell. Indeed, recent experiments verified that even coupling can be measured for an isolated element with negligible odd coupling, and under these experimental constraints, even coupling is given by its leading-order expression in Eq. (39) [50].

The dynamic features observed for *effective*, *equivalent*, and *Bloch* parameters are consistent with other numerical results in the published literature. When coupling parameters are included in the homogenization models of Willis [24] and Nemat-Nasser and Srivastava [25], the macroscopic compliance, inverse of stiffness C^{-1} in Eq. (3), and density both increase with increasing frequency, but when coupling parameters are absorbed into density and compliance (similar to the *equivalent* parameters), one of these slopes becomes negative, indicating a violation of causality. The homogenization model of Yang *et al.* [8] relies on reproducing surface fields and does not account for bianisotropy (similar to the *Bloch* parameters), and the results include parameters whose imaginary parts and slopes change sign, indicating causality and passivity violations.

The results of Sec. IV C demonstrate that even though *equivalent* and *Bloch* parameters are useful to describe wave

propagation in metamaterials, they do not always satisfy fundamental restrictions due to causality and passivity on macroscopic parameters and, therefore, these parameters lack physical meaning. This suggests that the *equivalent* and *Bloch* parameters may not be useful to describe the metamaterial response in the presence of more complex fields, such as in a resonator, and that the use of these parameters could unnecessarily complicate the interpretation of data from experiments or numerical simulations. Therefore, while all three of the models capture wave propagation in inhomogeneous media, one should expect that macroscopic parameters strictly obey reciprocity, causality, and passivity on their own, rather than in combination, to describe the overall response of inhomogeneous media.

V. CONCLUSIONS

This work provided a brief introduction to bianisotropy in electromagnetism and Willis coupling in elastodynamics in order to highlight physical analogies and promote a qualitative understanding of the origins of Willis coupling in acoustic metamaterials. The qualitative discussions were then verified by deriving a source-driven, self-consistent, multiple scattering homogenization procedure that highlighted the microscale and mesoscale origins of Willis coupling. The resulting *effective* parameters were then compared to two alternative macroscopic descriptions in light of physical constraints based on assumptions of passive and causal macroscopic wave propagation, which only the *effective* parameters satisfied. While it is meaningful to have parameters that satisfy physical restrictions, the direct determination of nonlocal effects is beyond the scope of current measurement techniques.

ACKNOWLEDGMENTS

C.F.S. and M.R.H. acknowledge support from ONR through MURI Grant No. N00014-13-1-0631, and A.A. acknowledges the support of NSF.

APPENDIX A: GREEN'S FUNCTIONS

The volumetric Dirac delta may be defined for 1D, 2D, and 3D space as

$$\delta_{\boldsymbol{n}} = \begin{cases} \delta(x-x_n)/A, & \text{1D} \\ \delta(x-x_n)\delta(y-y_n)/L_z, & \text{2D} \\ \delta(x-x_n)\delta(y-y_n)\delta(z-z_n), & \text{3D} \end{cases} \tag{A1}$$

where A is a representative cross-sectional area and L_z a representative out-of-plane length such that $\delta_{\boldsymbol{n}}$ has units of inverse volume in all three cases presented. The scalar free space Green's function in the reciprocal background medium $g(\boldsymbol{x}|\boldsymbol{x_n})$, which evaluates the scalar field at the point $\boldsymbol{x}$ due to a unit impulse at $\boldsymbol{x_n}$, is defined by $(\nabla^2 + k_0^2)g(\boldsymbol{x}|\boldsymbol{x_n}) = -\delta_{\boldsymbol{n}}$.

The fields due to body force $\boldsymbol{f}$ and mass source q distributions in a volume V are expressed in terms of the scalar Green's function as

$$\begin{aligned} \boldsymbol{u}(\boldsymbol{x}) &= -\frac{1}{i\omega\rho_0}\int_y \boldsymbol{f}(\boldsymbol{y})\cdot\nabla\nabla g(\boldsymbol{x}|\boldsymbol{y})dV \\ &\quad -\int_y q(\boldsymbol{y})\nabla g(\boldsymbol{x}|\boldsymbol{y})dV, \\ p(\boldsymbol{x}) &= -i\omega\rho_0\int_y q(\boldsymbol{y})g(\boldsymbol{x}|\boldsymbol{y})dV - \int_y \boldsymbol{f}(\boldsymbol{y})\cdot\nabla g(\boldsymbol{x}|\boldsymbol{y})dV. \end{aligned} \tag{A2}$$

From these expressions, the scattered fields at a point $\boldsymbol{x_m}$ due to an inhomogeneity located at $\boldsymbol{x_n}$ maybe expressed by Eq. (19) in terms of the dipole and monopole moments of the $\boldsymbol{n}$th inhomogeneity by relating the dipole moment to the body force $\boldsymbol{f} = i\omega\boldsymbol{d_n}\delta_{\boldsymbol{n}}$ and monopole moment to the volume source $q = -i\omega m_{\boldsymbol{n}}\delta_{\boldsymbol{n}}$. The modifed Green's functions are defined in Eq. (20).

The scalar Green's functions for 1D, 2D, and 3D are

$$g(\boldsymbol{x}|\boldsymbol{x_n}) = \begin{cases} ie^{ik_0|x-x_n|}/2k_0A, & \text{1D} \\ iH_0^{(1)}(k_0R_2)/4L_z, & \text{2D} \\ e^{ik_0R_3}/4\pi R_3, & \text{3D} \end{cases} \tag{A3}$$

where $H_0^{(1)}$ is the zero-order Hankel function of the first kind, $R_2 = \sqrt{(x-x_n)^2+(y-y_n)^2}$, and $R_3 = \sqrt{(x-x_n)^2+(y-y_n)^2+(z-z_n)^2}$. Then, for 1D, the modified Green's functions reduce to

$$\begin{aligned} \underline{\boldsymbol{G}}_{\mathrm{d}}^{\boldsymbol{mn}} &= \hat{x}\hat{x}\frac{ik_0}{2A}e^{ik_0L|m-n|} = \hat{x}\hat{x}G_{\mathrm{m}}^{\boldsymbol{mn}}, \\ \boldsymbol{G}_{\mathrm{c}}^{\boldsymbol{mn}} &= \pm\hat{x}\frac{ik_0}{2A}e^{ik_0L|m-n|}, \end{aligned} \tag{A4}$$

where $+\hat{x}$ corresponds to $m > n$ and $-\hat{x}$ to $m < n$.

APPENDIX B: SCATTERING MATRIX

Consider incident and outgoing acoustic waves at the boundaries of an inhomogeneity. The pressure amplitudes are related via the scattering matrix as

$$\begin{bmatrix} p_1^{\mathrm{out}} \\ p_2^{\mathrm{out}} \end{bmatrix} = \begin{bmatrix} S_{11} & S_{12} \\ S_{21} & S_{22} \end{bmatrix}\begin{bmatrix} p_1^{\mathrm{in}} \\ p_2^{\mathrm{in}} \end{bmatrix}, \tag{B1}$$

where the superscripts distinguish incident and outgoing and the subscripts indicate which boundary with p_1 evaluated at $x = -l/2$ and p_2 evaluated at $x = l/2$. A reciprocal inhomogeneity exhibits $S_{12} = S_{21}$, and if the inhomogeneity is also symmetric, then $S_{11} = S_{22}$. Outgoing waves may also be expressed in terms of incident and scattered pressures:

$$\begin{aligned} p_1^{\mathrm{out}} &= p_2^{\mathrm{in}}e^{ik_0l} + p_{\mathrm{s}}(-l/2) = S_{11}p_1^{\mathrm{in}} + S_{12}p_2^{\mathrm{in}}, \\ p_2^{\mathrm{out}} &= p_1^{\mathrm{in}}e^{ik_0l} + p_{\mathrm{s}}(l/2) = S_{21}p_1^{\mathrm{in}} + S_{22}p_2^{\mathrm{in}}. \end{aligned} \tag{B2}$$

In the absence of the inhomogeneity, local fields at $x = 0$ are given by the incident fields

$$\begin{aligned} p_{\mathrm{loc}} &= p_1^{\mathrm{in}}e^{ik_0l/2} + p_2^{\mathrm{in}}e^{ik_0l/2}, \\ \boldsymbol{u}_{\mathrm{loc}} &= \frac{\hat{x}}{Z_0}\left(p_1^{\mathrm{in}}e^{ik_0l/2} - p_2^{\mathrm{in}}e^{ik_0l/2}\right). \end{aligned} \tag{B3}$$

For 1D, evaluating Eq. (19) at $x = \pm l/2$ leads to

$$\begin{aligned} i\frac{k_0}{A}e^{ik_0 l/2}\frac{\boldsymbol{d_0}}{\rho_0} &= \boldsymbol{u}_s(l/2) + \boldsymbol{u}_s(-l/2), \\ -i\frac{k_0}{A}e^{ik_0 l/2}\frac{\boldsymbol{m_0}}{\beta_0} &= p_s(l/2) + p_s(-l/2). \end{aligned} \tag{B4}$$

The polarizablities may be determined using Eqs. (B2) and (B3) in Eq. (B4) to express the monopole and dipole moments in terms of local fields and comparing to Eq. (16).

APPENDIX C: INTERACTION COEFFICIENTS

Substituting the 1D modified Green's functions in Eq. (A4) into Eq. (23), the interaction coefficients become

$$\begin{aligned} C_m &= \frac{ik_0}{2A}\sum_{n=1}^{\infty}(e^{-i\boldsymbol{k}\cdot\hat{x}nL} + e^{i\boldsymbol{k}\cdot\hat{x}nL})e^{ik_0 nL}, \\ \underline{\boldsymbol{C}}_d &= \hat{x}\hat{x}\frac{ik_0}{2A}\sum_{n=1}^{\infty}(e^{-i\boldsymbol{k}\cdot\hat{x}nL} + e^{i\boldsymbol{k}\cdot\hat{x}nL})e^{ik_0 nL}, \\ \boldsymbol{C}_c &= \hat{x}\frac{ik_0}{2L}\sum_{n=1}^{\infty}(e^{-i\boldsymbol{k}\cdot\hat{x}nL} - e^{i\boldsymbol{k}\cdot\hat{x}nL})e^{ik_0 nL}. \end{aligned} \tag{C1}$$

Equation (34) may be obtained using the geometric series rule

$$\sum_{n=1}^{\infty}x^n = \frac{x}{1-x}, \tag{C2}$$

where $|x| < 1$. As discussed by Shore and Yaghjian [60], this approach is valid assuming some small imaginary part of $\boldsymbol{k}$ and k_0, i.e., damping, which is present in all real systems.

APPENDIX D: SCATTERED POWER RELATIONS

The derivation here is based on the work of Strickland *et al.* [72] for cylindrical scatterers. The restrictions on the complementary polarizabilities will be derived for a single inhomogeneity placed at the origin based on power conservation, i.e., the scattered power cannot exceed the power extracted from the local fields. The power extracted by the inhomogeneity must be positive and is given by

$$\begin{aligned} P_e &= -\frac{1}{2}\mathrm{Re}(i\omega\boldsymbol{d_0}\cdot\boldsymbol{u}^*_{\mathrm{loc}} + i\omega m^*_{\boldsymbol{0}}p_{\mathrm{loc}}) \\ &= \frac{\omega}{2}\mathrm{Im}(\boldsymbol{d_0}\cdot\boldsymbol{u}^*_{\mathrm{loc}} + m^*_{\boldsymbol{0}}p_{\mathrm{loc}}), \end{aligned} \tag{D1}$$

which for 1D and using Eq. (21) simplifies to

$$P_e = -\frac{\omega}{2}[d_0 \quad m_0]\cdot\begin{bmatrix}\frac{\mathrm{Im}(\tilde{\alpha}_d)}{\rho_0} & \frac{\mathrm{Im}(\tilde{\alpha}_c)}{-i/c_0} \\ \frac{\mathrm{Im}(\tilde{\alpha}_c)}{i/c_0} & \frac{\mathrm{Im}(\tilde{\alpha}_m)}{\beta_0}\end{bmatrix}\cdot\begin{bmatrix}d_0 \\ m_0\end{bmatrix}^*. \tag{D2}$$

The total power radiated from the inhomogeneity, determined from the scattered fields, Eq. (19), may be expressed as

$$\begin{aligned} P_r &= \frac{1}{2}\mathrm{Re}(-p_s\boldsymbol{u}^*_s|_{x=-l/2} + p_s\boldsymbol{u}^*_s|_{x=l/2})\cdot\hat{x}A \\ &= \frac{\omega}{2}\frac{k_0}{2A}[d_0 \quad m_0]\cdot\begin{bmatrix}1/\rho_0 & 0 \\ 0 & 1/\beta_0\end{bmatrix}\cdot\begin{bmatrix}d_0 \\ m_0\end{bmatrix}^*. \end{aligned} \tag{D3}$$

For a passive inhomogeneity, $P_e \geqslant P_r$, which leads to $\mathrm{Im}(\tilde{\alpha}_d) \leqslant -k_0/2A$ and $\mathrm{Im}(\tilde{\alpha}_m) \leqslant -k_0/2A$, where equality only occurs for a lossless inhomogeneity, and $\mathrm{Im}(\tilde{\alpha}_c) = 0$ for a lossless inhomogeneity. Additionally, since $P_e - P_r \geqslant 0$, the matrix

$$\begin{bmatrix}-\left(\frac{k_0}{2A} + \mathrm{Im}(\tilde{\alpha}_d)\right)/\rho_0 & -ic_0\mathrm{Im}(\tilde{\alpha}_c) \\ ic_0\mathrm{Im}(\tilde{\alpha}_c) & -\left(\frac{k_0}{2A} + \mathrm{Im}(\tilde{\alpha}_m)\right)/\beta_0\end{bmatrix}$$

must be positive definite, requiring

$$\mathrm{Im}(\tilde{\alpha}_c)^2 \leqslant \left(\frac{k_0}{2A} + \mathrm{Im}(\tilde{\alpha}_d)\right)\left(\frac{k_0}{2A} + \mathrm{Im}(\tilde{\alpha}_m)\right). \tag{D4}$$

[1] J. R. Willis, in *Continuum Micromechanics: CISM Courses and Lectures No. 377*, edited by P. Suquet (Springer, New York, 1997), pp. 265–290.
[2] D. R. Smith, D. C. Vier, N. Kroll, and S. Schultz, Appl. Phys. Lett. **77**, 2246 (2000).
[3] D. R. Smith and J. B. Pendry, J. Opt. Soc. Am. B **23**, 391 (2006).
[4] C. Fietz and G. Shvets, Proc. SPIE **7392**, 73920L (2009).
[5] A. Alù, Phys. Rev. B **84**, 075153 (2011).
[6] J. R. Willis, Proc. R. Soc. A **467**, 1865 (2011).
[7] A. N. Norris, A. L. Shuvalov, and A. A. Kutsenko, Proc. R. Soc. A **468**, 1629 (2012).
[8] M. Yang, G. Ma, Y. Wu, Z. Yang, and P. Sheng, Phys. Rev. B **89**, 064309 (2014).
[9] D. Torrent, Y. Pennec, and B. Djafari-Rouhani, Phys. Rev. B **92**, 174110 (2015).
[10] M. A. Gorlach, T. A. Voytova, M. Lapine, Y. S. Kivshar, and P. A. Belov, Phys. Rev. B **93**, 165125 (2016).
[11] M. B. Muhlestein and M. R. Haberman, Proc. R. Soc. A **472**, 20160438 (2016).
[12] C. R. Simovski, J. Opt. **13**, 013001 (2011).
[13] A. Alù, Phys. Rev. B **83**, 081102 (2011).
[14] M. B. Muhlestein, C. F. Sieck, A. Alù, and M. R. Haberman, Proc. R. Soc. A **472**, 20160604 (2016).
[15] D. K. Cheng and J.-A. Kong, Proc. IEEE **56**, 248 (1968).
[16] J. A. Kong, Proc. IEEE **60**, 1036 (1972).
[17] I. V. Lindell, A. H. Sihvola, S. A. Tretyakov, and A. J. Viitanen, *Electromagnetic Waves in Chiral and Bi-isotropic Media* (Artech House, Boston, 1994), pp. 1–22.
[18] J. R. Willis, Int. J. Solids Struct. **21**, 805 (1985).
[19] G. W. Milton and J. R. Willis, Proc. R. Soc. A **463**, 855 (2007).
[20] A. Lakhtakia, V. K. Varadan, and V. V. Varadan, *Time-Harmonic Electromagnetic Fields in Chiral Media* (Springer, New York, 1989), pp. 1–5, 100–107.
[21] V. V. Varadan, A. Lakhtakia, and V. K. Varadan, J. Wave-Mater. Interact. **1**, 315 (1986).
[22] M. M. I. Saadoun and N. Engheta, Microw. Opt. Technol. Lett. **5**, 184 (1992).
[23] D. A. Powell and Y. S. Kivshar, Appl. Phys. Lett. **97**, 091106 (2010).

[24] J. R. Willis, Mech. Mater. **41**, 385 (2009).
[25] S. Nemat-Nasser and A. Srivastava, J. Mech. Phys. Solids **59**, 1953 (2011).
[26] H. Nassar, Q.-C. He, and N. Auffray, J. Mech. Phys. Solids **77**, 158 (2015).
[27] S. Koo, C. Cho, J.-h. Jeong, and N. Park, Nat. Commun. **7**, 13012 (2016).
[28] *Extending the Theory of Composites to Other Areas of Science*, edited by G. Milton (Milton-Patton, Salt Lake City, UT, 2016), pp. 29–30.
[29] C. F. Sieck, A. Alù, and M. R. Haberman, Phys. Procedia **70**, 275 (2015).
[30] M.-F. Ponge, O. Poncelet, and D. Torrent, Extreme Mech. Lett. **12**, 71 (2017).
[31] B. D. H. Tellegen, Philips Research Reports **3**, 81 (1948).
[32] L.-Q. Shui, Z.-F. Yue, Y.-S. Liu, Q.-C. Liu, J.-J. Guo, and X.-D. He, Compos. Sci. Technol. **113**, 19 (2015).
[33] H. Nassar, X. Xu, A. N. Norris, and G. L. Huang, J. Mech. Phys. Solids **101**, 10 (2017).
[34] J. D. Jackson, *Classical Electrodynamics*, 3rd ed. (Wiley, New York, 1998).
[35] P. E. Doak, Theor. Comput. Fluid Dyn. **10**, 115 (1998).
[36] F. Guérin, Prog. Electromagn. Res. **9**, 31 (1994).
[37] K. F. Lindman, Finska Vet. Soc. Öfversigt **57**, A.3 (1914).
[38] M. M. I. Saadoun and N. Engheta, Prog. Electromagn. Res. **9**, 351 (1994).
[39] D. Ramaccia, L. D. Palma, D. Ates, E. Ozbay, A. Toscano, and F. Bilotti, IEEE Trans. Antennas Propag. **62**, 2093 (2014).
[40] A. A. Andronov, Izv. Vyssh. Uchebn. Zaved., Radiofiz **3**, 645 (1960).
[41] V. P. Silin, Sov. Phys.–JETP **11**, 703 (1960) [J. Exp. Theor. Phys. **38**, 977 (1960)].
[42] G. Kluge and G. Scholz, Acta Acust. united Ac. **16**, 60 (1965).
[43] D. L. Portigal and E. Burstein, Phys. Rev. **170**, 673 (1968).
[44] A. S. Pine, Phys. Rev. B **2**, 2049 (1970).
[45] K. F. Tee, A. Spadoni, M. Scarpa, and F. Ruzzene, ASME J. Vib. Acoust. **132**, 031007 (2010).
[46] R. Wunenburger, J. I. V. Lozano, and E. Brasselet, New J. Phys. **17**, 103022 (2015).
[47] J. R. Willis, J. Mech. Phys. Solids **28**, 287 (1980).
[48] J. R. Willis, Wave Motion **3**, 1 (1981).
[49] A. Srivastava, Int. J. Smart Nano Mater. **6**, 41 (2015).
[50] M. B. Muhlestein, C. F. Sieck, P. S. Wilson, and M. R. Haberman, Nat. Commun. **8**, 15625 (2017).
[51] G. W. Milton, New J. Phys. **9**, 359 (2007).
[52] I. Lindell, *Methods for Electromagnetic Field Analysis* (Clarendon, New York, 1992), pp. 57, 89–95.
[53] L. D. Landau and E. M. Lifshitz, *Electrodynamics of Continuous Media* (Pergamon, New York, 1960), pp. 253–268.
[54] T. Koschny, P. Markoš, D. R. Smith, and C. M. Soukoulis, Phys. Rev. E **68**, 065602 (2003).
[55] D. T. Blackstock, *Fundamentals of Physical Acoustics* (Wiley, New York, 2000), pp. 65–98, 511–512.
[56] F. V. Hunt, J. Acoust. Soc. Am. **27**, 1019 (1955).
[57] V. Twersky, J. Acoust. Soc. Am. **36**, 1314 (1964).
[58] V. Twersky, J. Acoust. Soc. Am. **64**, 1710 (1978).
[59] D. Torrent and J. Sánchez-Dehesa, New J. Phys. **13**, 093018 (2011).
[60] R. A. Shore and A. D. Yaghjian, Radio Sci. **42**, RS6S21 (2007).
[61] D. M. Pozar, *Microwave Engineering*, 3rd ed. (Wiley, New York, 2004), pp. 174–185, 371–378.
[62] A. Alù, A. D. Yaghjian, R. A. Shore, and M. G. Silveirinha, Phys. Rev. B **84**, 054305 (2011).
[63] L. Brillouin, *Wave Propagation in Periodic Structures: Electric Filters and Crystal Lattices* (Dover, New York, 2003), pp. 80–85.
[64] A. A. Kutsenko, A. L. Shuvalov, O. Poncelet, and A. N. Darinskii, J. Acoust. Soc. Am. **137**, 606 (2015).
[65] V. Fokin, M. Ambati, C. Sun, and X. Zhang, Phys. Rev. B **76**, 144302 (2007).
[66] F. Bongard, H. Lissek, and J. R. Mosig, Phys. Rev. B **82**, 094306 (2010).
[67] Y. M. Seo, J. J. Park, S. H. Lee, C. M. Park, C. K. Kim, and S. H. Lee, J. Appl. Phys. **111**, 023504 (2012).
[68] C. E. Bradley, J. Acoust. Soc. Am. **96**, 1844 (1994).
[69] C. E. Bradley, J. Acoust. Soc. Am. **96**, 1854 (1994).
[70] A. Srivastava and S. Nemat-Nasser, Wave Motion **51**, 1045 (2014).
[71] N. Fang, D. Xi, J. Xu, M. Ambati, W. Srituravanich, C. Sun, and X. Zhang, Nat. Mater. **5**, 452 (2006).
[72] D. Strickland, A. Ayón, and A. Alù, Phys. Rev. B **91**, 085104 (2015).